iScience

CellPress

Article

Coupling of DNA Replication and Negative Feedback Controls Gene Expression for Cell-Fate Decisions

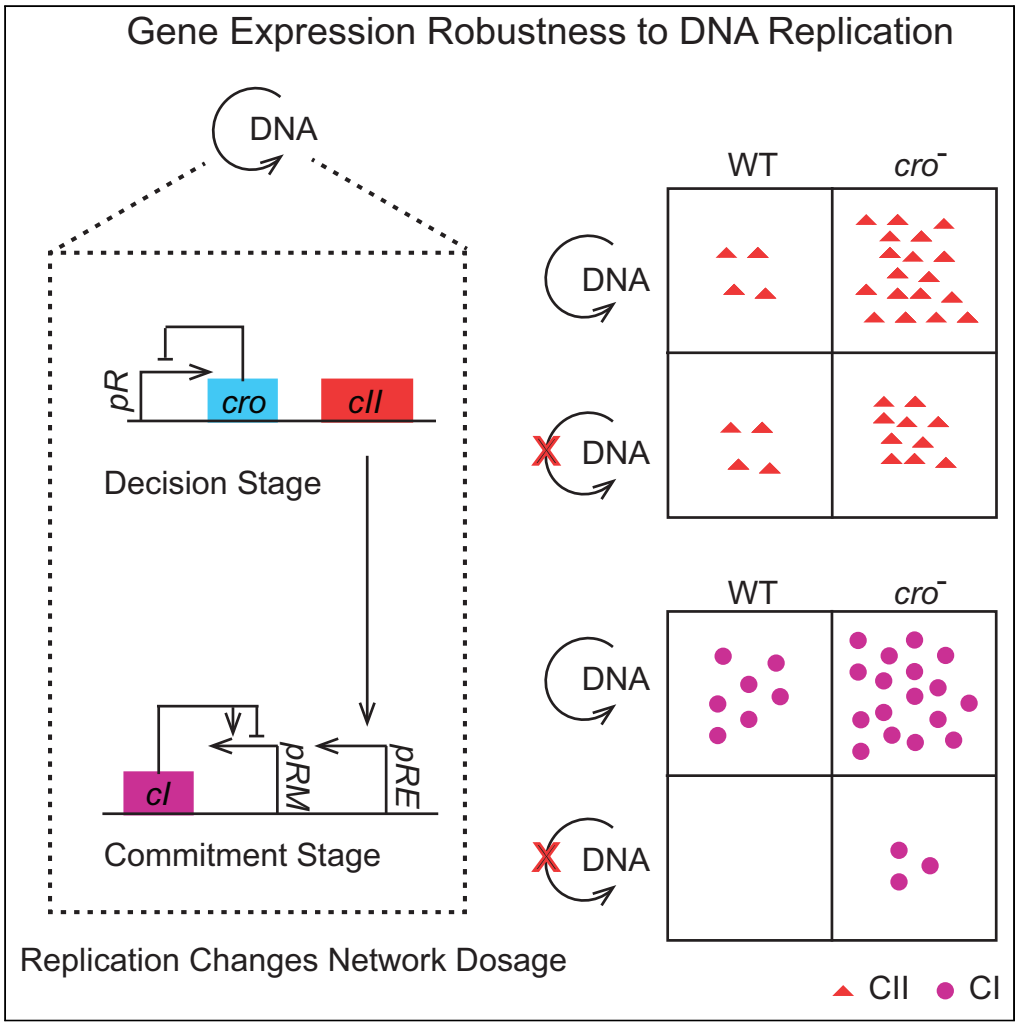

Qiuyan Shao, Michael G. Cortes, Jimmy T. Trinh, Jingwen Guan, Gábor Balázsi, Lanying Zeng

gabor.balazsi@stonybrook.edu (G.B.)
lzeng@tamu.edu (L.Z.)

HIGHLIGHTS

One single DNA is not able to commit to either lytic or lysogenic decision

DNA replication increases lysogenization frequency by boosting *cI* expression

CII expression is robust to DNA copy number changes resulting from DNA replication

Robustness of CII expression is due to Cro negative feedback

Shao et al., iScience 6, 1–12
August 31, 2018
https://doi.org/10.1016/j.isci.2018.07.006

iScience

CellPress

Article

Coupling of DNA Replication and Negative Feedback Controls Gene Expression for Cell-Fate Decisions

Qiuyan Shao,[1,2,7] Michael G. Cortes,[3,4,7] Jimmy T. Trinh,[1,2] Jingwen Guan,[2,5] Gábor Balázsi,[3,6,*] and Lanying Zeng[1,2,5,8,*]

SUMMARY

Cellular decision-making arises from the expression of genes along a regulatory cascade, which leads to a choice between distinct phenotypic states. DNA dosage variations, often introduced by replication, can significantly affect gene expression to ultimately bias decision outcomes. The bacteriophage lambda system has long served as a paradigm for cell-fate determination, yet the effect of DNA replication remains largely unknown. Here, through single-cell studies and mathematical modeling we show that DNA replication drastically boosts *cI* expression to allow lysogenic commitment by providing more templates. Conversely, expression of CII, the upstream regulator of *cI*, is surprisingly robust to DNA replication due to the negative autoregulation of the Cro repressor. Our study exemplifies how living organisms can not only utilize DNA replication for gene expression control but also implement mechanisms such as negative feedback to allow the expression of certain genes to be robust to dosage changes resulting from DNA replication.

INTRODUCTION

Cellular decision-making often relies on the output of its gene regulatory networks, which are sensitive to intra- and extracellular signals (Balazsi et al., 2011; Perkins and Swain, 2009). In some cases, the gene network senses and responds to these signals by up- or downregulating the expression levels of certain genes to optimize the organism's survival (Kramer, 2010). In other cases, however, it is preferable for the cell's phenotype to remain insensitive (robust) to perturbations (Alon et al., 1999; Stelling et al., 2004; von Dassow et al., 2000). There are a great variety of perturbations that gene networks must mitigate, such as changes in physical conditions (e.g., temperature), the abundance of environmental toxins or nutrients, and the fluctuation of intracellular protein and toxin levels. In particular, one such perturbation to gene networks is DNA copy number fluctuation (e.g., by DNA replication), which virtually all living organisms must experience. Gene copy number changes can potentially affect gene expression to cause significant phenotypic changes (Baumgart et al., 2017; Kemkemer et al., 2002; Pollack et al., 2002; Rancati et al., 2008; Seidman and Seidman, 2002). For example, highly amplified genes in cancer cells often show elevated expression (Pollack et al., 2002), whereas inactivation of a single allele in diploid organisms can reduce expression and lead to diseases (Seidman and Seidman, 2002). Theoretical modeling also reveals that a number of commonly observed gene regulatory subnetworks, or network motifs, are sensitive to gene copy number changes due to interactions via a common pool of transcription factors in the duplicated networks (Mileyko et al., 2008).

Organisms can also develop strategies to deal with gene dosage changes and their cognate effects. A recent study reveals that in budding yeast, *Saccharomyces cerevisiae*, the expression of a large fraction of genes is significantly reduced when the gene dosage is halved, whereas some genes have unaltered expression (Springer et al., 2010). This suggests that there may exist mechanisms and control structures keeping a small number of genes robust to gene dosage variations. Indeed, some studies have reported network structures allowing gene expression insensitivity to DNA dosage changes (Acar et al., 2010; Song et al., 2014). However, those observations are most often based on gene deletions or insertions, and the effects of replication-associated temporal DNA copy number changes remain largely unknown. Given the prevalence of DNA replication and the fluctuation of DNA levels during cell growth, it is natural to ask how gene networks can cope with or take advantage of DNA replication to choose the optimal cell fate.

[1]Department of Biochemistry and Biophysics, Texas A&M University, College Station, TX 77843, USA

[2]Center for Phage Technology, Texas A&M University, College Station, TX 77843, USA

[3]The Louis and Beatrice Laufer Center for Physical and Quantitative Biology, Stony Brook University, Stony Brook, NY, USA

[4]Department of Applied Mathematics and Statistics, Stony Brook University, Stony Brook, NY, USA

[5]Molecular and Environmental Plant Science, Texas A&M University, College Station, TX 77843, USA

[6]Department of Biomedical Engineering, Stony Brook University, Stony Brook, NY, USA

[7]These authors contributed equally

[8]Lead Contact

*Correspondence: gabor.balazsi@stonybrook.edu (G.B.), lzeng@tamu.edu (L.Z.)

https://doi.org/10.1016/j.isci.2018.07.006

To understand the effect of DNA copy number fluctuations on gene expression and network level outputs, we use phage lambda as a model system to study how ongoing viral replication affects the lysis-lysogeny decision. The genetic components involved in this lysis-lysogeny decision have been well-characterized (Hendrix, 1983; Oppenheim et al., 2005; Ptashne, 2004). The default lytic pathway for lambda infection is executed by the transcription and translation of the lysis and phage morphological genes, which lead to the bursting of the cell and release of hundreds of phage progeny. These events are triggered when the anti-terminator protein, Q, reaches a threshold, allowing transcription from promoter pR′ to bypass the downstream terminator, tR′ (Cortes et al., 2017; Kobiler et al., 2005; Roberts et al., 1998). The alternative lysogenic pathway culminates in the integration of phage DNA into the *E. coli* chromosome, and the inhibition of gene transcription from the two major promoters pR and pL by repressor CI (Oppenheim et al., 2005). The master viral regulator, CII, plays a central role in controlling CI production by activating the pRE promoter. The choice between lytic and lysogenic development is therefore shaped by the cascade of regulatory genes expressed early in the infection process. After a decision is made, it is enforced by CI to establish the lysogenic pathway, or by cell destruction through lysis to complete the lytic pathway. Phage DNA replication starts shortly after the infection, causing a radical change in DNA copy number concordant with the expression of lysis-lysogeny decision-making genes. Here, we examine the effect of gene dosage change on the expression of two highly important decision regulators, CII and CI.

An alternative source of DNA copy number variation in the lambda infection system is the different MOI (Multiplicity of Infection, or number of infecting phages per cell), which determines the initial concentration of intracellular phage DNA. Current experimental evidence and theoretical models of phage lambda suggest that lysogenization is preferred at a higher MOI, i.e., higher initial DNA concentration (Cortes et al., 2017; Joh and Weitz, 2011; Kourilsky, 1973; Weitz et al., 2008; Zeng et al., 2010). A deterministic model of the CI/Cro bistable switch predicts that a high CI, low Cro state becomes the dominant attractor state when viral concentration is high (Weitz et al., 2008) because higher MOI leads to a higher transient spike in CII levels, causing an overshoot of CI via CII activation of the pRE promoter. This allows the CI/Cro bistable switch to flip to the direction of high CI and low Cro levels even if Cro was initially high, consistent with the lysogenic development (Kobiler et al., 2005). A quasi-stochastic version of this model indicated that this trend holds true even if lytic and lysogenic decisions are determined by threshold crossing of Q and CI, respectively, as opposed to steady state attractors (Joh and Weitz, 2011). Notably, these two models kept the viral DNA level constant throughout the dynamics by leaving out DNA replication, and just varied the infection MOI. Later, DNA replication was introduced in other models, which suggests that DNA replication promotes lysogeny by increasing DNA concentration similar to higher MOI (Cortes et al., 2017; Robb and Shahrezaei, 2014). However, thorough experimental interrogation of the regulation of decision-making by DNA replication is still lacking.

In this work, we experimentally characterize the role of DNA replication in the lysis-lysogeny decision of lambda phage and discover that CII levels remain robust to DNA replication, especially during the early infection period. Combined with mathematical modeling, our work suggests that negative feedback by Cro plays an important role in keeping CII expression robust to DNA replication. On the contrary, expression of *cI*, the downstream target gene of *cII*, is extremely sensitive to DNA copy number variations, thereby affecting the lysis-lysogeny decisions. Overall, we show that different elements of a gene network respond distinctly to copy number variations and demonstrate the potential of negative feedback regulation to encode phenotypic robustness against extremely variable DNA copy numbers.

RESULTS

Lack of DNA Replication Leads to Failure in Lytic and Lysogenic Development

To understand how DNA replication may affect the lysis-lysogeny decision, we studied phage infection outcomes in the absence of replication. For this, we investigated how the DNA replication-defective λ*P*⁻ mutant (see Transparent Methods and Tables S1–S4 for more strain information) differs in its ability to make decisions compared with the wild-type (WT) laboratory strain λWT. The lysogenization frequency of λ*P*⁻ has been reported (Kourilsky, 1973) to be lower than that of λWT at low APIs (average phage input, calculated as plaque-forming unit [PFU]/colony-forming unit [CFU]). We confirmed this earlier finding (Figure S1A). In addition, the lysogenic response (percentage of lysogeny) of λ*P*⁻ phage to API follows a Poisson distribution of $n \geq 3$, indicating that lysogenization requires 3 or more λ*P*⁻ phages on average, compared with $n \geq 2$ for λWT (Figure S1B). This suggests that lysogenic decisions are possible in the absence of DNA replication, but more initial phage inputs are required to cause the same level of lysogenization.

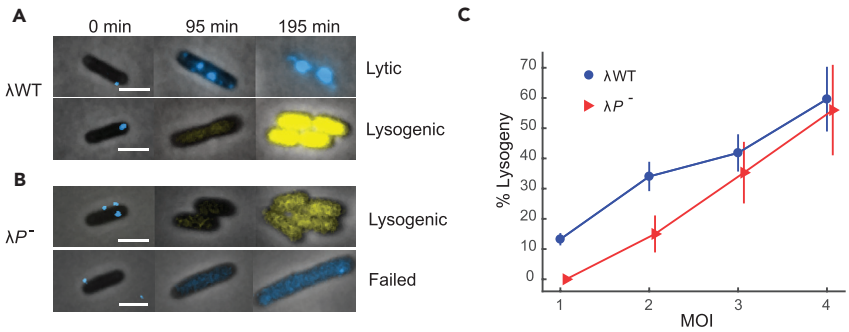

Figure 1. More than One Copy of Phage DNA Is Required for Lysogenic Establishment

(A) Representative images showing lytic and lysogenic events by λWT. Top: a cell is apparently infected by one λWT phage (blue dot at 0 min), and subsequently gpD-mTurquoise2 expression (blue) is observed. Cell lysis is observed at 195 min. Bottom: a cell is apparently infected by one λWT phage (blue dot at 0 min). *cI* reporter expression (yellow) and cell division are observed, indicating a successful lysogenization event.

(B) Representative images of lysogenic and failed infection by λ*P*⁻. Top: a cell is apparently infected by 3 λ*P*⁻ phages (blue dots at 0 min). The cell divides, and expression of the *cI* reporter (yellow) is observed, indicating lysogenization. Bottom: a cell is apparently infected by one λ*P*⁻ phage (blue dot at 0 min). The cell does not divide, and only minimal expression of gpD-mTurquoise2 is detected, indicating that the phage failed to reach either the lytic or lysogenic decision.

(C) Lysogenization frequency of λWT and λ*P*⁻. For both phages, the lysogenization frequency increases with MOI. λ*P*⁻ has lower lysogenization frequencies at MOI $\leq$ 3, and reaches a similar level at MOI = 4. At MOI = 1, no lysogenization events (0 of 35 infections) are observed for λ*P*⁻. Error bars denote SEM.

Scale bars denote 2 μm. See also Figures S1 and S2.

To quantitatively detect the differences in decision-making behaviors in the presence and absence of phage DNA replication, we utilized our established lytic-lysogenic reporter systems (Trinh et al., 2017) to study the decision-making of λ*P*⁻ phage at the single-cell/single-phage level. Briefly, a fluorescent protein (mKO2) is inserted downstream of *cI* on the phage genome to report *cI* transcription activity, corresponding to lysogenic events by λWT infections (Figures 1A and S2). Another fluorescent protein (mTurquoise2) was fused to the C terminus of the phage capsid decoration protein, gpD. Thus, mTurquoise2 fluorescence reports lytic development up until host cell lysis for λWT infections (Figure 1A). This method also allows the quantification of MOI for each infection (Figure 1A, blue dot at 0 min). Overall, the λ*P*⁻ phage lysogenized less frequently than λWT (Figure 1C), as predicted by bulk experiments (Figure S1). Remarkably, λ*P*⁻ phage infections showed no lysogenic events at MOI = 1 (Figure 1C, 0 of 35 cells). In the lysogenic cells of MOI > 1, the *cI* reporter signal was lower than in λWT infections (Figures 1A and 1B), suggesting that *cI* transcription levels are lower in the absence of DNA replication. In addition, DNA replication is also required for cell lysis, as we only observed very low levels of the lytic reporter expression (Figure 1B). Accordingly, lysis did not occur within the time window of our time-lapse movies (4 hr) as opposed to λWT, where cells lysed at 114 $\pm$ 16 min (mean $\pm$ SD, N = 243). Overall, our data suggest that the decision-making network outputs, CI and the lysis genes, are severely compromised in the absence of DNA replication. The expression of these genes is regulated by their corresponding transcription factors, CII and Q, respectively. Therefore, we next sought to quantify how DNA replication affects the expression of these transcription factors from the pR promoter using single-molecule fluorescence *in situ* hybridization (smFISH).

Single-Molecule Characterization of pR Transcription Activity after Phage Infection

Most of the key lysis-lysogeny-determining genes, including *cII* and *Q*, are located on the pR transcript (Figure 2A). Therefore, to determine the overall expression of cellular decision-controlling regulators, we quantified the level of pR transcription at the single-cell level using smFISH (see Transparent Methods and Table S5 for more details), by targeting the *cII* gene and its neighboring region, as an initial step to uncover the molecular mechanism of the decision-making process. In these experiments, we controlled the MOI by infecting with an API of 0.1–0.2. As the distribution of the number of phage particles per cell follows a Poisson distribution (Zeng et al., 2010), the estimated percentages of infected cells (cells with $\geq$1 infecting phages) at an API of 0.1 and 0.2 were 9.5% and 18.1%, respectively. Correspondingly, the estimated percentages of MOI = 1 infections within infected cells were 95.1% and 90.3%. Indeed, we observed that the percentage of cells showing *cII* signals ranges from 10.8% to 15.2% in multiple

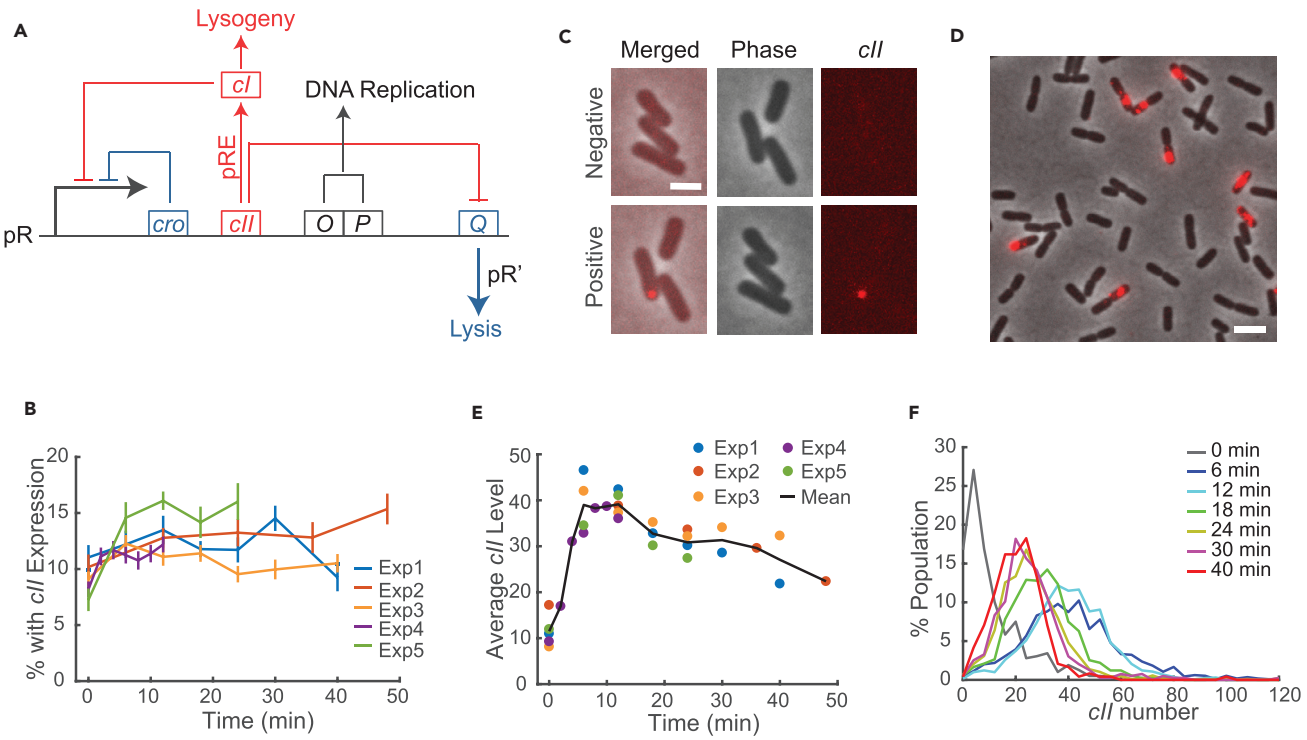

Figure 2. Schematic of Lambda Lysis-Lysogeny Decision-Making and the Characterization of *cII* mRNA Expression

(A) The pR transcript includes the *cro*, *cII*, *O*, *P*, and *Q* genes. Cro and CI both repress the pR promoter. O and P are required for phage DNA replication. CII activates the expression of CI from the pRE promoter, whereas it represses Q through paQ. Q allows transcription of the lysis and morphogenesis genes from pR′.

(B) Percentage of cells showing *cII* expression after infection. Data from multiple experiments were shown. A plateau is reached after 2 min of infection, when samples were taken every 2 min (Exp4). Overall, between 10.8% (Exp3, averaged over 6–40 min) and 15.2% (Exp5, averaged over 6–24 min) of the cells show *cII* expression in multiple experiments, consistent with an API of 0.1–0.2. Error bars denote SEM.

(C) Representative images showing cells from the negative and positive samples. Top: cells without phage infection. None of the cells show *cII* signal. Bottom: cells with λWT infection at API = 0.2. Images were taken at 0 min. One cell shows a distinct focus (red). The other two cells do not show foci either because they have not started the mRNA expression, or they are not infected.

(D) Representative images showing *cII* mRNA expression at 6 min. *cII* mRNA appeared as clusters instead of punctate foci.

(E) Average *cII* levels (calculated as the average of all cells pooled from all 5 experiments) over time after λWT infection. Data from multiple experiments (dots) and the mean (black line) are shown. Only infected cells with *cII* expression were included in the calculation. *cII* expression reaches a peak at around 6–12 min after infection and subsequently drops.

(F) Distribution of *cII* mRNA levels at different time points. Combined data from Exp1, Exp3, and Exp5 (as in panels D and E) are shown. The *cII* mRNA distributions at 6 and 12 min are similar and gradually shift to the lower end after 18 min.

Scale bars denote 2 μm. See also Figures S3 and S4.

experiments (Figure 2B), indicating that the infection API is within the range of 0.1–0.2. Under these experimental conditions, most infections are at an MOI of 1. This minimized the effect of MOI, an important factor affecting the lysogenization frequency (Kourilsky, 1973), and therefore allowed us to focus on the role of DNA replication for cell-fate decisions by one single infecting phage. At 0 min after λWT phage infection, a small fraction of cells displayed one *cII* focus (Figure 2C), which likely corresponds to one single mRNA or a few mRNAs clustering together. At later time points, i.e., 6 min as shown in Figure 2D, the *cII* mRNA clusters become larger and brighter, indicating that *cII* mRNA level increases in cells over time. The percentage of cells showing *cII* transcription quickly reaches a plateau within the first 2 min of infection, indicating that gene expression closely follows phage infection (Figure 2B). To validate our mRNA detection method, we quantified the mRNA numbers from smFISH (see details in Transparent Methods and Figure S3) and then compared the average expression levels with data obtained by qRT-PCR. The data obtained from the two methods were in good agreement (Figure S4). Overall, the average *cII* mRNA level quickly peaked at around 6–12 min after infection, and subsequently dropped (Figure 2E), reflecting the repression of pR promoter by either CI or Cro (Kobiler et al., 2005; Oppenheim et al., 2005). Moreover, *cII* levels in different cells

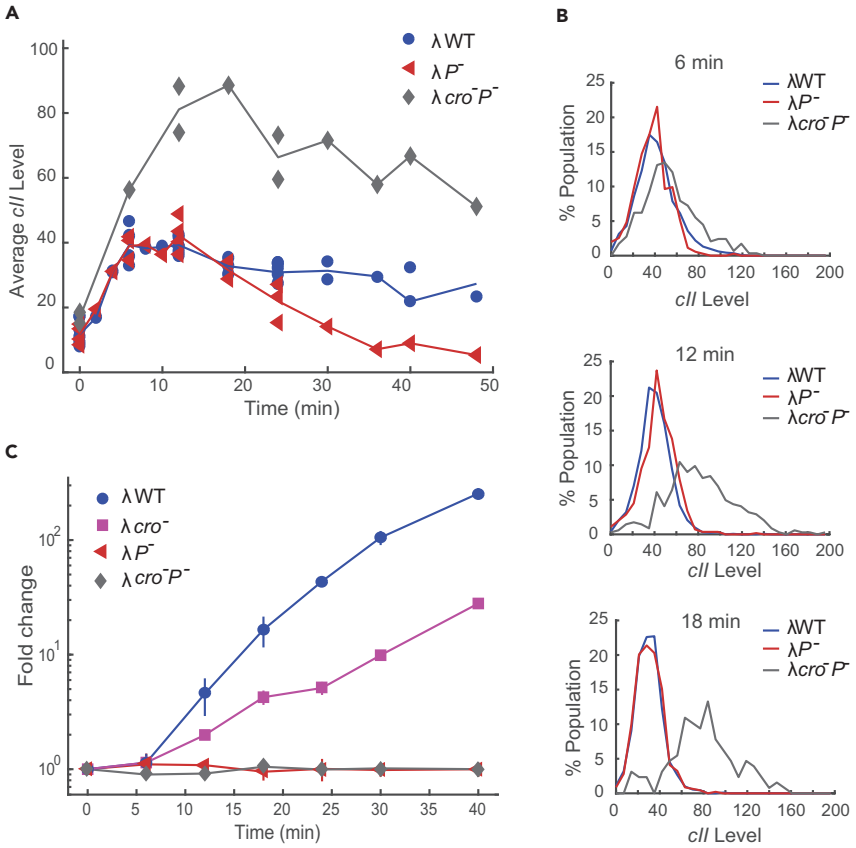

Figure 3. Early *cII* Expression Is Not Affected by DNA Replication

(A) Average *cII* levels comparing λWT, λP^-, and λcro^-P^- infections. Data from multiple experiments are shown, and solid lines represent the mean of all cells pooled from different experiments. In the first 18 min, λWT and λP^- have similar *cII* levels. After 24 min of infection, average λWT *cII* level is higher compared with λP^-. Average *cII* expression for λcro^-P^- infection is higher throughout the infection.

(B) Distribution of *cII* mRNA levels at 6, 12, and 18 min after infection. λWT and λP^- have similar *cII* distributions, whereas λcro^-P^- infection shows higher *cII* expression levels.

(C) Average DNA level after infection. Fold change is calculated as the ratio of phage DNA to *E. coli* DNA normalized to time 0 and further normalized to the mean of λP^- and λcro^-P^- data at the corresponding time point. For λWT and λcro^- infection, phage DNA level increases by 256 ± 7-fold and 29 ± 5-fold, respectively, after 40 min of infection. Error bars denote SEM. See also Figure S5.

showed a wide population distribution (Figure 2F). For example, at 6 min, the number of *cII* molecules per cell has a mean of 38.8 and a coefficient of variation of 0.47.

cII Expression Is Robust to Gene Dosage Changes Arising from DNA Replication

Having validated the smFISH method under our experimental settings, we proceeded to investigate the effect of DNA replication on the expression of transcription factor *cII*. Unexpectedly, λWT and λP^- displayed similar levels of *cII* mRNA expression on average, especially through the first 18 min (Figure 3A). As these smFISH experiments were performed in lysogeny broth (LB) medium, where cell lysis typically occurs at ~60 min and lysogenic decisions are reached within the first 20 min, the data suggest that *cII* expression is not affected by DNA replication in the time window when lysogenic decisions are processed. After 24 min, the *cII* level for λWT remains higher, whereas λP^- seems to drop more rapidly and reach a lower level (Figure 3A). The reasons for the difference in *cII* level at the late time points can be complicated as different decisions are reached and different feedback regulations are in place. We therefore focused on the early time points (0–18 min) and asked if *cII* expression dynamics are altered in the absence of DNA replication to result in the decreased lysogenic frequency that we observed through live-cell movies (Figure 1C) and bulk

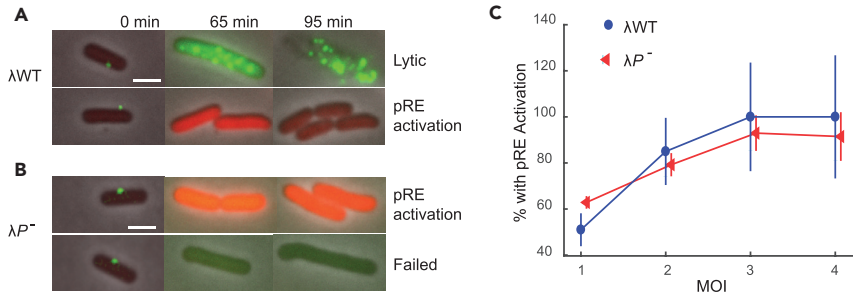

Figure 4. Normal pRE Activation without DNA Replication

(A) Representative images of lytic and lysogenic events by λWT infections at MOI = 1. Top: expression of gpD-EYFP (green) is observed and the cell lyses at 95 min. Bottom: increase of mCherry (red) expression and normal cell division is observed, indicating a successful lysogenic event.

(B) Representative images showing λP^- infections at MOI = 1. Top: increase in mCherry expression is observed, indicating the activation of pRE promoter. Low levels of gpD-EYFP expression are also detected in the cell. Bottom: only a very low level of gpD-EYFP expression is observed. Division is inhibited, and the cell keeps growing longer without lysing. Same contrast was applied to the images in (A) and (B) at 65 and 95 min. At 0 min, a different contrast if applied to see the green phage particles.

(C) Percentages of cells with pRE activation at different MOIs. Both phages show similar levels of pRE activation at different MOIs. Error bars denote SEM.

Scale bars denote 2 μm.

lysogenic assays (Figure S1A). Surprisingly, we did not observe significant differences in the distribution of *cII* mRNA between λWT and λP^- either (Figure 3B).

To rule out the possibility that phage DNA replication simply does not occur until after 18 min, we quantified the phage DNA level using qPCR. As shown in Figure 3C (see Transparent Methods and Figure S5 for more details), the relative number of phage DNA to *E. coli* genome increases by 16.5 ± 5 (mean ± SEM) fold at 18 min after λWT infection, indicating that phages undergo a substantial amount of DNA replication within this time frame. On the contrary, λP^- infection had no detectable replication, as expected (Figure 3C). Altogether, our results suggest that *cII* expression is robust to the gene dosage variations resulting from DNA replication during the early infection time window.

Having shown that λP^- infection leads to the same levels of *cII* mRNA expression during the decision-making time window, we next wanted to confirm that the CII protein concentration in the λP^- strain is also sufficient for the activation of the pRE promoter. We used a multi-copy plasmid, pRE-*mCherry*, to report the activation of pRE promoter by CII (Kobiler et al., 2005; Zeng et al., 2010). This system artificially increases the copy number of pRE promoter without affecting the decision-making of λWT phage (Zeng et al., 2010). We used EYFP-labeled fluorescent phages (green dots in Figures 4A and 4B) to quantify the MOI. We found that at MOI = 1, 62.9% (N = 835) of λP^- and 50.5% (N = 101) of λWT infections were able to activate this reporter (Figure 4), further confirming that a single λP^- DNA is capable of producing a sufficient amount of CII protein to activate the pRE promoter, an essential step in establishing lysogeny. In fact, the percentage activation by λP^- was slightly higher than that of λWT infections, which might be due to additional effects of DNA replication on the expression of other genes that also affect the decision outcomes.

cI Expression Responds Strongly to Gene Dosage Changes Arising from DNA Replication

So far, our data suggest that the main effect of DNA replication during phage lysogenization is on downstream processes of *cII* expression. To understand why the lack of DNA replication decreases the lysogenic frequency, we next compared *cI* expression in the presence and absence of DNA replication. By simultaneously detecting *cII* and *cI* mRNA, we found that whereas 33.4 ± 1.7% (averaged over time points 24, 36, and 48 min, with N = 152, 126, and 152, respectively) λWT-infected cells show *cI* expression, very few λP^--infected cells (0, 1, 2, 0, and 0 out of N = 62, 157, 111, 102, and 61 cells at time points 0, 12, 24, 36, and 48 min, respectively) express *cI* mRNA at API ≤ 0.2 (Figure 5A). Moreover, in those rarely observed *cI*-expressing cells infected by λP^-, the expression level is very low (≤2 *cI* mRNA per cell), confirming a severe deficiency in *cI* expression in the absence of DNA replication.

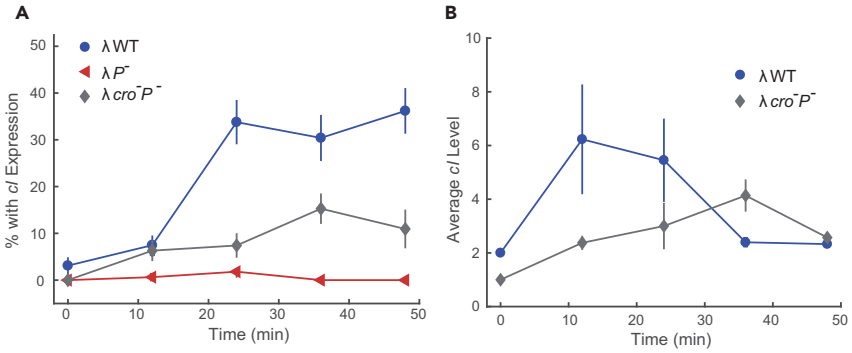

Figure 5. Low *cI* Expression without DNA Replication

(A) Percentage of infected cells with *cI* expression. After 24 min, 33.4 ± 1.7% (averaged over 24, 36 and 48 min) of λWT infection leads to *cI* expression, which is higher than λ*cro*⁻*P*⁻. Frequency of *cI* expression in λ*P*⁻ infection is very low. Error bars denote SEM.

(B) Comparison of average *cI* expression level. Only cells with *cI* expression are included for calculation. *cI* level for λWT peaks at around 12–24 min. λ*cro*⁻*P*⁻ has delayed *cI* peak time at 40 min with a lower peak level. Error bars denote SEM. See also Figure S1.

To further dissect the mechanism of lysogenic establishment, we tested a λ*cro*⁻*P*⁻ double mutant. Due to the absence of the repressor Cro, this double mutant has much higher *cII* mRNA levels compared with λWT (Figures 3A and 3B). With this mutant, we characterized how a single phage DNA responds to elevated *cII* levels. We found that cells infected by this mutant phage showed *cI* mRNA expression less frequently, despite having higher *cII* levels than the λWT infections (Figure 5A). The average *cI* expression level for λ*cro*⁻*P*⁻ is also lower (Figure 5B), suggesting that this phage cannot effectively carry out the lysogenic decision despite having ample expression of *cII*. Our bulk lysogenization assay also showed that λ*cro*⁻*P*⁻ does not lysogenize as frequently as λWT (Figure S1C). Altogether, the data suggest that CII is not the only key factor regulating *cI* expression and lysogenic decisions, and that a single phage DNA is generally incompetent at consummating lysogeny. An increase in DNA copy number is important to enable the production of additional *cI* transcripts to boost CI levels.

Cro Negative Feedback Enables *cII* Expression Robustness against Replication-Associated Gene Dosage Variations

To systematically understand how the viral gene network encodes *cII* robustness to viral DNA replication, we computationally simulated the network behavior in the infection process by adapting a published model (Cortes et al., 2017). This model includes the key components of the decision-making network, namely, Cro, CI, and CII and their interactions, as well as DNA replication (Figures 2A and S6, Tables S6 and S7). The goal of the model is to capture the important behaviors of the true network, not to account for all of its known features. This model simulates transcription of pR mRNA, which is then translated into CII and Cro proteins. CII activates the pRE promoter, driving the transcription and translation of the *cI* gene. We phenomenologically modeled the repression of the pR promoter by CI and Cro using Hill functions (Cortes et al., 2017; Joh and Weitz, 2011; Robb and Shahrezaei, 2014; Weitz et al., 2008). Likewise, we used Hill functions to model the CI activation and Cro repression of pRM promoter. As we focused on the early decision-making phase of infection when CI is not highly expressed, we did not include the CI repression on pRM promoter for simplicity. We also modeled viral DNA replication and its effects on CI, CII, and Cro expression. Lastly, we phenomenologically modeled the repression of CI on DNA replication using a Hill function. The *cII* expression level predicted by this model agreed closely with the experimental data (Figure 6A), indicating that the interactions in the model were sufficient to capture the robustness of CII levels to DNA replication. We have also built a more complex model where the binding and unbinding reactions of transcription factors to their cognate promoters are simulated in detail. This model has similar performance to the simplified model that we presented above (see Transparent Methods, Figure S7, Tables S8 and S9 and Data S1 for more details), therefore, only the results of the simplified model will be further discussed here.

We next sought to understand which network features or components give rise to the *cII* expression robustness to DNA replication. Examining this network, we found two network features regulating pR mRNA

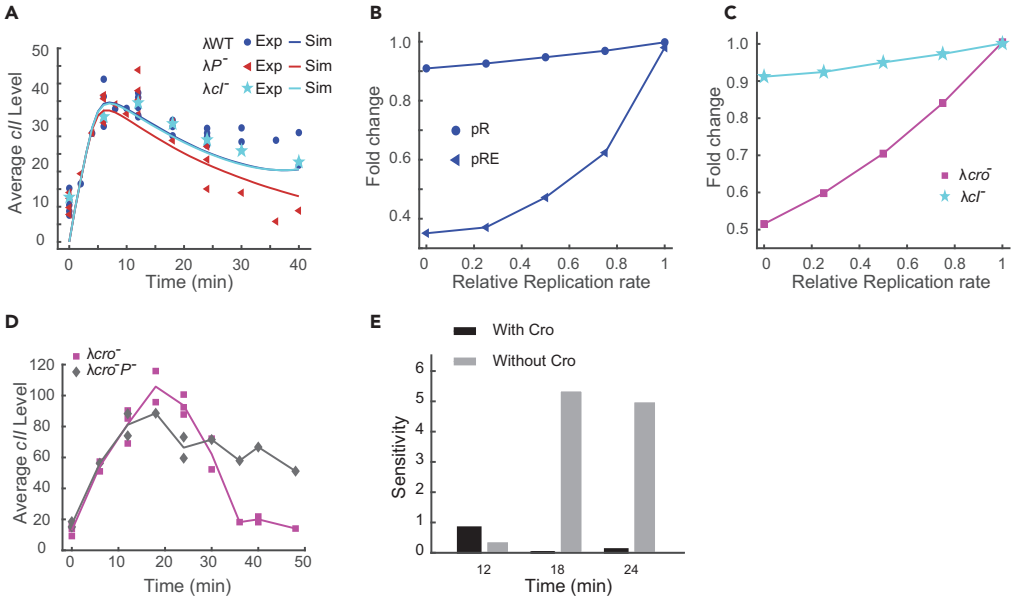

Figure 6. Cro Is Important for the Robustness of *cII* Expression to DNA Replication

(A) The model prediction of the mean *cII* level in comparison with the experimental data. The model captures the average *cII* expression for λWT, λP^-, and λcI^-. Both experimental quantification and model prediction show that λcI^- mutant has similar *cII* expression levels to λWT and λP^- at the early infection period (0–20 min).

(B) Model prediction of the relative pR and pRE mRNA levels under different replication rates. Under the model assumptions, pR transcription level shows minimal changes as the replication rate varies between 0- and 1-fold of the original replication rate, whereas the pRE level varies greatly, agreeing with experimental observations.

(C) Model prediction of the sensitivity of pR mRNA levels for λcro^- and λcI^- mutants. Removing Cro from the model gives rise to pR transcription sensitivity to DNA replication, whereas removing CI does not cause significant changes.

(D) Experimental validation of the role of Cro in *cII* expression robustness to DNA replication. In the cro^- background, removing DNA replication (λcro^-P^-) causes a decrease of *cII* level at 18 and 24 min.

(E) *cII* expression sensitivity to DNA replication. The sensitivity is calculated as the absolute difference in *cII* level between λWT and λP^- (with Cro) or λcro^- and λcro^-P^- (without Cro) at each time point divided by the DNA number difference within each group. In the absence of Cro, the *cII* expression sensitivity to DNA replication greatly increases, as shown at 18 and 24 min.

See also Figures S6 and S7.

transcription: the Cro negative feedback regulation and CI negative feedback regulation (Figure 2A). Negative feedback is a network motif that has been shown to possess properties such as reducing gene expression noise and linearizing gene expression level to the input signal (Becskei and Serrano, 2000; Nevozhay et al., 2009). To determine whether any of these two negative feedback regulatory links alone is responsible for *cII* mRNA expression robustness, we systematically removed the effect of CI and Cro on pR transcription and DNA replication to generate computational mutants with compromised feedback regulation. To examine the sensitivity of mRNA expression to different rates of DNA replication for the various computational mutants, we first calculated for each time point t from 6 to 24 min the average fold change, $F(\varepsilon, t)$, defined as the ratio of mRNA levels at replication rate $\varepsilon \cdot r$ (for $0 \leq \varepsilon \leq 1$) versus mRNA levels at the WT replication rate r. Then, we calculated the time-average of this quantity, $F(\varepsilon)$, to get the sensitivity over all time points. In the WT background, the model successfully predicted the *cII* expression robustness to DNA replication (Figure 6B). Moreover, CI removal did not compromise the robustness of *cII* expression to a wide range of replication rates (Figure 6C). On the contrary, removing Cro significantly increases the sensitivity of *cII* expression to DNA replication (Figure 6C), indicating the importance of Cro for the robustness of *cII* expression to DNA replication.

To validate these theoretical predictions, we then experimentally probed the expression of *cII* in different mutant backgrounds. As expected, *cII* expression was similar among the λcI^-, λP^-, and λWT infections (Figure 6A), suggesting that CI is not essential for *cII* expression robustness under our experimental settings. We further tested the role of Cro negative feedback by comparing *cII* expression level between λcro^- and

λ*cro*$^-$*P*$^-$. As shown in Figure 6D, λ*cro*$^-$*P*$^-$ infection leads to lower *cII* levels at 18 and 24 min compared with λ*cro*$^-$. As the replication rate of λ*cro*$^-$ phage is lower compared with λWT, we then calculated the *cII* expression sensitivity as the mean *cII* level change per extra DNA (Figure 6E), which indicated robustness. Altogether, our data suggest that Cro can overcome the variations of gene dosages to result in *cII* expression robustness. To understand the difference between the contributions of CI and Cro to the *cII* expression robustness, we examined the timing and expression of CI versus Cro. CI is only expressed in cells entering the lysogenic state (33.4% for λWT at MOI = 1, Figure 5A), whereas Cro is present in all cells. Moreover, by the time DNA replication starts (~6 min), there is most likely a substantial amount of Cro present already, since Cro is one of the first two genes to be expressed during infection. On the contrary, *cI* expression only starts when CII protein reaches a certain threshold. It is therefore possible that the different contributions of CI and Cro to *cII* expression robustness are due to their difference in the timing and magnitude of expression, yet further experimentation is needed to provide more support.

DISCUSSION

The lysis-lysogeny decision-making of bacteriophage lambda has long served as a paradigm for studying stochastic cell-fate selection, due to the well-established genetic networks involved (Oppenheim et al., 2005). Following decades of studies, researchers have characterized the effects of most genetic components (Hendrix, 1983) and built models to understand this process systematically (Arkin et al., 1998; Joh and Weitz, 2011; Weitz et al., 2008). However, due to the limit of resolution in previous experimental approaches, the effect of DNA copy number changes resulting from DNA replication on the decision-making process has been largely neglected, which may have obscured important aspects of this process. Here, we provided more quantitative measurements of their effects on gene expression, decision-making, and the enforcement of the cell-fate decisions.

Gene expression and DNA replication are both partly stochastic processes (Elowitz et al., 2002; Kaern et al., 2005; Raj and van Oudenaarden, 2008), and in the lambda network, DNA replication and the expression of genes, such as Cro, can affect each other. O and P, proteins required for phage DNA replication, are under the control of pR promoter, and their expression is affected by Cro and CI. In addition, replication initiation seems to require active pR transcription (Dove et al., 1969; Mensa-Wilmot et al., 1989), whereas Cro and CI both repress pR promoter activities. On the other hand, pR transcription goes in the opposite direction of DNA replication, originating from λ*ori* located at the *O* gene region. As head-on collisions between transcription and replication have been shown to slow replication (Merrikh et al., 2012; Pomerantz and O'Donnell, 2010; Soultanas, 2011), pR transcription and phage DNA replication might be constantly affecting each other as well. This dynamic interplay may have interesting impacts on the level of gene expression and DNA replication. Due to the limit of our experimental approaches, we cannot follow the copy number changes of phage DNA simultaneously with the expression of genes. As a result, the exact cellular concentrations of phage DNA and *cII* and *cI* mRNAs at the time of lysogenic establishment are unknown. Future experiments with higher resolutions are needed to allow the examination of the correlations of DNA copy number with cell-fate selection.

Increasing the copy number of promoters can titrate transcription factors and lead to complex dosage response (Lee and Maheshri, 2012; Rydenfelt et al., 2014). Using a simple repression regulatory architecture, researchers have found that at a high transcription factor:promoter ratio, the gene expression response is similar to that of a single isolated copy of the gene (Brewster et al., 2014). Networks invariant to gene dosage have also been reported. In *Saccharomyces cerevisiae*, the activity of the galactose signaling network (GAL network) was invariant to the network dosage changes when the gene copy number was halved (Acar et al., 2010). The finding was further generalized by mathematical simulations to conclude that for any N-component network, containing a 2-component subnetwork with an activator, an inhibitor, as well as a 1:1 stoichiometry interaction between the activator and inhibitor is both necessary and sufficient for the network to be dosage compensated (Acar et al., 2010; Song et al., 2014). An alternative mechanism that provides robustness to DNA copy number changes is an incoherent feedforward loop with DNA copy number as its source node (Segall-Shapiro et al., 2018).

Notably, in these studies, the copy number changes are usually introduced through deletion and insertion of genes, or changing the plasmid copy numbers, and it is possible that the effects of dosage variations resulting from DNA replication can be different. In the lambda system, both MOI and DNA replication affect decision-making by affecting the DNA concentration, although the response of *cII* expression to

these two factors seems to be different. Experimentation and theoretical modeling have suggested that the difference might be due to Cro. Specifically, increasing the MOI leads to the introduction of more copies of DNA into a cell in which Cro is not present yet. On the contrary, by the time DNA replication starts, Cro has been expressed to a certain level such that negative feedback by Cro counteracts the effect of increasing template number on *cII* expression.

Strategies such as negative feedback are commonly utilized by gene regulatory networks to increase gene expression stability (Becskei and Serrano, 2000), or to linearize the input-output response of the genes (Nevozhay et al., 2009). By reducing the gene expression noise, networks can achieve more ordered, "deterministic" outcomes, as reliability is important for many cellular processes. For phage lambda, as a repressor, Cro has been shown to perform multiple important roles in the development of the lytic pathway (Court et al., 2007; Johnson et al., 1978; Ptashne et al., 1980; Svenningsen et al., 2005). Interestingly, by artificially inserting Cro onto the *E. coli* chromosome and placing Cro under the control of pR with one single operator binding site, oR1 (as opposed to three: oR1, oR2, and oR3, in the native lambda genome), researchers observed oscillations of Cro expression, synchronized to the cell cycle and the associated gene copy changes (Hensel and Marquez-Lago, 2015). However, the period of these oscillations were several fold longer than the time frame of lambda phage decision-making right after infection. Here, our work suggests that Cro-mediated negative feedback can stabilize the activity of the pR promoter against DNA copy number variations resulting from DNA replication, thus creating conditions wherein the early decision-making process is not affected by DNA replication. Since Cro plays two major roles in the network, both to repress pR promoter activity and to modulate the rate of DNA replication, these two functions may seem convoluted in providing *cII* expression robustness. However, it is hard to decouple the two roles of Cro both experimentally and theoretically due to the complex interplay between Cro and DNA replication as discussed. Future work to elucidate the mechanism of regulation on DNA replication by Cro as well as the development of mutants to separate the two functions of Cro will be of great interest.

Whether or not transcription factor expression robustness to network dosage changes confers any evolutionary advantages to the lambda decision-making circuit remains unknown. Due to the different physiological state or growth phase of the host cell, the levels of DNA replication may be different in different cells. The resource level, i.e., the available DNA polymerase, may fluctuate in response to different environmental stimuli to result in changes in the rate of DNA replication. To address these potential changes, lambda seems to adapt by allowing its effector (*cI*) expression to respond to the DNA copy number changes rather than altering the actual decision-making (*cII* expression) behavior. Recent studies showed that dosage-compensating networks can act as a noise reduction module to reduce the effects of extrinsic noise on the network output (Peng et al., 2016). In the lambda system, the behavior of the decision-making circuit in response to fluctuations in different cellular factors remain unknown.

Overall, our study has shown that the lambda decision-making process is composed of an intricate network where both MOI changes and replicating DNA can significantly affect the outcomes. However, the lambda network is far more complicated than what we described here. CIII is also an important factor for lysogenic establishment by promoting CII stability (Herman et al., 1997; Hoyt et al., 1982), and its expression might also be affected by DNA replication, yet it is neglected in our models for simplicity. The anti-terminator N is critical for phage development by allowing the transcription to go beyond N and Cro production at the immediately early stage, and possibly regulates the temporal progression of gene expression as well as decision-making (Oppenheim et al., 2005). On the other hand, the fate-determining genes on the pR transcript, although promoted from the same promoter, are in fact separated by several terminators, tR1–4 (Casjens and Hendrix, 2015; Oppenheim et al., 2005). Although N can allow transcription to go past those terminators, the efficiencies may vary (Gusarov and Nudler, 2001). This adds another layer of regulation, and a more systematic examination of gene expression is required to fully understand the lambda decision-making network.

METHODS

All methods can be found in the accompanying Transparent Methods supplemental file.

SUPPLEMENTAL INFORMATION

Supplemental Information includes Transparent Methods, seven figures, nine tables, and one data file and can be found with this article online at https://doi.org/10.1016/j.isci.2018.07.006.

ACKNOWLEDGMENTS

We are grateful to Ryland Young and Chenxi Qiu for commenting on the earlier versions of the manuscript. We thank Ryland Young and Donald Court for gifting strains, and Ido Golding, Samuel O Skinner, Leonardo A. Sepulveda, and Mengyu Wang for helpful suggestions on the smFISH experiments and data analysis. This research was supported by NIH-NIGMS grant R01GM107597 and Administrative Supplement 3R01GM107597-02S1 to L.Z. and G.B., as well as by NIH-NIGMS grant R35GM122561 and by a Laufer Center for Physical and Quantitative Biology endowment to G.B.

AUTHOR CONTRIBUTIONS

Q.S., J.T.T., and L.Z. designed the experiments. Q.S., J.T.T., and J.G. conducted the experiments. Q.S. and J.T.T. analyzed the data. M.G.C., Q.S., and G.B. built the mathematical models. Q.S., M.G.C., J.T.T., G.B., and L.Z. wrote the paper. G.B. and L.Z. supervised the project.

DECLARATION OF INTERESTS

The authors declare no competing interests.

Received: April 24, 2018
Revised: May 21, 2018
Accepted: July 9, 2018
Published: August 31, 2018

REFERENCES

Acar, M., Pando, B.F., Arnold, F.H., Elowitz, M.B., and van Oudenaarden, A. (2010). A general mechanism for network-dosage compensation in gene circuits. Science *329*, 1656–1660.

Alon, U., Surette, M.G., Barkai, N., and Leibler, S. (1999). Robustness in bacterial chemotaxis. Nature *397*, 168–171.

Arkin, A., Ross, J., and McAdams, H.H. (1998). Stochastic kinetic analysis of developmental pathway bifurcation in phage lambda-infected Escherichia coli cells. Genetics *149*, 1633–1648.

Balazsi, G., van Oudenaarden, A., and Collins, J.J. (2011). Cellular decision making and biological noise: from microbes to mammals. Cell *144*, 910–925.

Baumgart, L., Mather, W., and Hasty, J. (2017). Synchronized DNA cycling across a bacterial population. Nat. Genet. *49*, 1282–1285.

Becskei, A., and Serrano, L. (2000). Engineering stability in gene networks by autoregulation. Nature *405*, 590–593.

Brewster, R.C., Weinert, F.M., Garcia, H.G., Song, D., Rydenfelt, M., and Phillips, R. (2014). The transcription factor titration effect dictates level of gene expression. Cell *156*, 1312–1323.

Casjens, S.R., and Hendrix, R.W. (2015). Bacteriophage lambda: early pioneer and still relevant. Virology *479-480*, 310–330.

Cortes, M.G., Trinh, J.T., Zeng, L., and Balazsi, G. (2017). Late-arriving signals contribute less to cell-fate decisions. Biophys. J. *113*, 2110–2120.

Court, D.L., Oppenheim, A.B., and Adhya, S.L. (2007). A new look at bacteriophage lambda genetic networks. J. Bacteriol. *189*, 298–304.

Dove, W.F., Hargrove, E., Ohashi, M., Haugli, F., and Guha, A. (1969). Replicator activation in lambda. Jpn. J. Genet. *44*, 11–22.

Elowitz, M.B., Levine, A.J., Siggia, E.D., and Swain, P.S. (2002). Stochastic gene expression in a single cell. Science *297*, 1183–1186.

Gusarov, I., and Nudler, E. (2001). Control of intrinsic transcription termination by N and NusA: the basic mechanisms. Cell *107*, 437–449.

Hendrix, R.W. (1983). Lambda II (Cold Spring Harbor Laboratory).

Hensel, Z. and Marquez-Lago, T.T. (2015). Cell-cycle-synchronized, oscillatory expression of a negatively autoregulated gene in E. coli. q-bioQM, arXiv:1506.08596v1.

Herman, C., Thevenet, D., D'Ari, R., and Bouloc, P. (1997). The HflB protease of Escherichia coli degrades its inhibitor lambda cIII. J. Bacteriol. *179*, 358–363.

Hoyt, M.A., Knight, D.M., Das, A., Miller, H.I., and Echols, H. (1982). Control of phage lambda development by stability and synthesis of cII protein: role of the viral cIII and host hflA, himA and himD genes. Cell *31*, 565–573.

Joh, R.I., and Weitz, J.S. (2011). To lyse or not to lyse: transient-mediated stochastic fate determination in cells infected by bacteriophages. PLoS Comput. Biol. *7*, e1002006.

Johnson, A., Meyer, B.J., and Ptashne, M. (1978). Mechanism of action of the cro protein of bacteriophage lambda. Proc. Natl. Acad. Sci. USA *75*, 1783–1787.

Kaern, M., Elston, T.C., Blake, W.J., and Collins, J.J. (2005). Stochasticity in gene expression: from theories to phenotypes. Nat. Rev. Genet. *6*, 451–464.

Kemkemer, R., Schrank, S., Vogel, W., Gruler, H., and Kaufmann, D. (2002). Increased noise as an effect of haploinsufficiency of the tumor-suppressor gene neurofibromatosis type 1 in vitro. Proc. Natl. Acad. Sci. USA *99*, 13783–13788.

Kobiler, O., Rokney, A., Friedman, N., Court, D.L., Stavans, J., and Oppenheim, A.B. (2005). Quantitative kinetic analysis of the bacteriophage lambda genetic network. Proc. Natl. Acad. Sci. USA *102*, 4470–4475.

Kourilsky, P. (1973). Lysogenization by bacteriophage lambda. I. Multiple infection and the lysogenic response. Mol. Gen. Genet. *122*, 183–195.

Kramer, R. (2010). Bacterial stimulus perception and signal transduction: response to osmotic stress. Chem. Rec. *10*, 217–229.

Lee, T.H., and Maheshri, N. (2012). A regulatory role for repeated decoy transcription factor binding sites in target gene expression. Mol. Syst. Biol. *8*, 576.

Mensa-Wilmot, K., Carroll, K., and McMacken, R. (1989). Transcriptional activation of bacteriophage lambda DNA replication in vitro: regulatory role of histone-like protein HU of Escherichia coli. EMBO J. *8*, 2393–2402.

Merrikh, H., Zhang, Y., Grossman, A.D., and Wang, J.D. (2012). Replication-transcription conflicts in bacteria. Nat. Rev. Microbiol. *10*, 449–458.

Mileyko, Y., Joh, R.I., and Weitz, J.S. (2008). Small-scale copy number variation and large-scale changes in gene expression. Proc. Natl. Acad. Sci. USA *105*, 16659–16664.

Nevozhay, D., Adams, R.M., Murphy, K.F., Josic, K., and Balazsi, G. (2009). Negative autoregulation linearizes the dose-response and

suppresses the heterogeneity of gene expression. Proc. Natl. Acad. Sci. USA *106*, 5123–5128.

Oppenheim, A.B., Kobiler, O., Stavans, J., Court, D.L., and Adhya, S. (2005). Switches in bacteriophage lambda development. Annu. Rev. Genet. *39*, 409–429.

Peng, W., Song, R., and Acar, M. (2016). Noise reduction facilitated by dosage compensation in gene networks. Nat. Commun. *7*, 12959.

Perkins, T.J., and Swain, P.S. (2009). Strategies for cellular decision-making. Mol. Syst. Biol. *5*, 326.

Pollack, J.R., Sorlie, T., Perou, C.M., Rees, C.A., Jeffrey, S.S., Lonning, P.E., Tibshirani, R., Botstein, D., Borresen-Dale, A.L., and Brown, P.O. (2002). Microarray analysis reveals a major direct role of DNA copy number alteration in the transcriptional program of human breast tumors. Proc. Natl. Acad. Sci. USA *99*, 12963–12968.

Pomerantz, R.T., and O'Donnell, M. (2010). What happens when replication and transcription complexes collide? Cell Cycle *9*, 2537–2543.

Ptashne, M. (2004). Genetic Switch: Phage Lambda Revisited (Cold Spring Harbor Laboratory Press).

Ptashne, M., Jeffrey, A., Johnson, A.D., Maurer, R., Meyer, B.J., Pabo, C.O., Roberts, T.M., and Sauer, R.T. (1980). How the lambda repressor and cro work. Cell *19*, 1–11.

Raj, A., and van Oudenaarden, A. (2008). Nature, nurture, or chance: stochastic gene expression and its consequences. Cell *135*, 216–226.

Rancati, G., Pavelka, N., Fleharty, B., Noll, A., Trimble, R., Walton, K., Perera, A., Staehling-Hampton, K., Seidel, C.W., and Li, R. (2008). Aneuploidy underlies rapid adaptive evolution of yeast cells deprived of a conserved cytokinesis motor. Cell *135*, 879–893.

Robb, M.L., and Shahrezaei, V. (2014). Stochastic cellular fate decision making by multiple infecting lambda phage. PLoS One *9*, e103636.

Roberts, J.W., Yarnell, W., Bartlett, E., Guo, J., Marr, M., Ko, D.C., Sun, H., and Roberts, C.W. (1998). Antitermination by bacteriophage lambda Q protein. Cold Spring Harb. Symp. Quant. Biol. *63*, 319–325.

Rydenfelt, M., Cox, R.S., 3rd, Garcia, H., and Phillips, R. (2014). Statistical mechanical model of coupled transcription from multiple promoters due to transcription factor titration. Phys. Rev. E Stat. Nonlin. Soft Matter Phys. *89*, 012702.

Segall-Shapiro, T.H., Sontag, E.D., and Voigt, C.A. (2018). Engineered promoters enable constant gene expression at any copy number in bacteria. Nat. Biotechnol. *36*, 352–358.

Seidman, J.G., and Seidman, C. (2002). Transcription factor haploinsufficiency: when half a loaf is not enough. J. Clin. Invest. *109*, 451–455.

Song, R., Liu, P., and Acar, M. (2014). Network-dosage compensation topologies as recurrent network motifs in natural gene networks. BMC Syst. Biol. *8*, 69.

Soultanas, P. (2011). The replication-transcription conflict. Transcription *2*, 140–144.

Springer, M., Weissman, J.S., and Kirschner, M.W. (2010). A general lack of compensation for gene dosage in yeast. Mol. Syst. Biol. *6*, 368.

Stelling, J., Sauer, U., Szallasi, Z., Doyle, F.J., and Doyle, J. (2004). Robustness of cellular functions. Cell *118*, 675–685.

Svenningsen, S.L., Costantino, N., Court, D.L., and Adhya, S. (2005). On the role of Cro in lambda prophage induction. Proc. Natl. Acad. Sci. USA *102*, 4465–4469.

Trinh, J.T., Szekely, T., Shao, Q., Balazsi, G., and Zeng, L. (2017). Cell fate decisions emerge as phages cooperate or compete inside their host. Nat. Commun. *8*, 14341.

von Dassow, G., Meir, E., Munro, E.M., and Odell, G.M. (2000). The segment polarity network is a robust developmental module. Nature *406*, 188–192.

Weitz, J.S., Mileyko, Y., Joh, R.I., and Voit, E.O. (2008). Collective decision making in bacterial viruses. Biophys. J. *95*, 2673–2680.

Zeng, L., Skinner, S.O., Zong, C., Sippy, J., Feiss, M., and Golding, I. (2010). Decision making at a subcellular level determines the outcome of bacteriophage infection. Cell *141*, 682–691.

ISCI, Volume *6*

Supplemental Information

Coupling of DNA Replication and Negative Feedback Controls Gene Expression for Cell-Fate Decisions

Qiuyan Shao, Michael G. Cortes, Jimmy T. Trinh, Jingwen Guan, Gábor Balázsi, and Lanying Zeng

Supplemental figures and legends

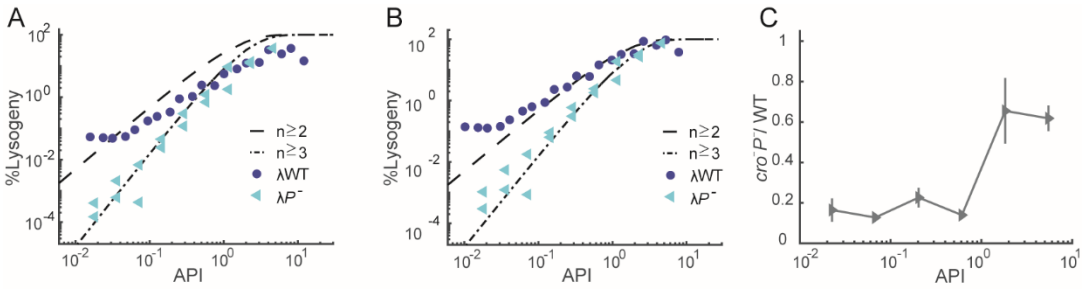

Figure S1. DNA replication is important for lambda lysogenization. Related to Figure 1C and Figure 5A.

(A) The lysogenization frequency of cells after λWT and λ*P*⁻ infections at different APIs. Combined data of two experiments are shown. The λ*P*⁻ phage infection leads to lower lysogenization frequencies at the low APIs, and has the same level as λWT at high APIs.

(B) The data from (A) were shifted to fit into the curves of Poisson distribution. λWT follows the Poisson distribution of n≥2, indicating that 2 or more phages are required to lysogenize the cell on average. λ*P*⁻ follows n≥3, indicating that the lack of DNA replication leads to different patterns of lysogenic response.

(C) At high APIs, λWT phage has only slightly higher lysogenization frequencies compared to that of λ*cro*⁻*P*⁻. As API drops, the lysogenization frequency of λ*cro*⁻*P*⁻ is only 0.16 ± 0.06 fold of λWT. Error bars denote standard error of the mean.

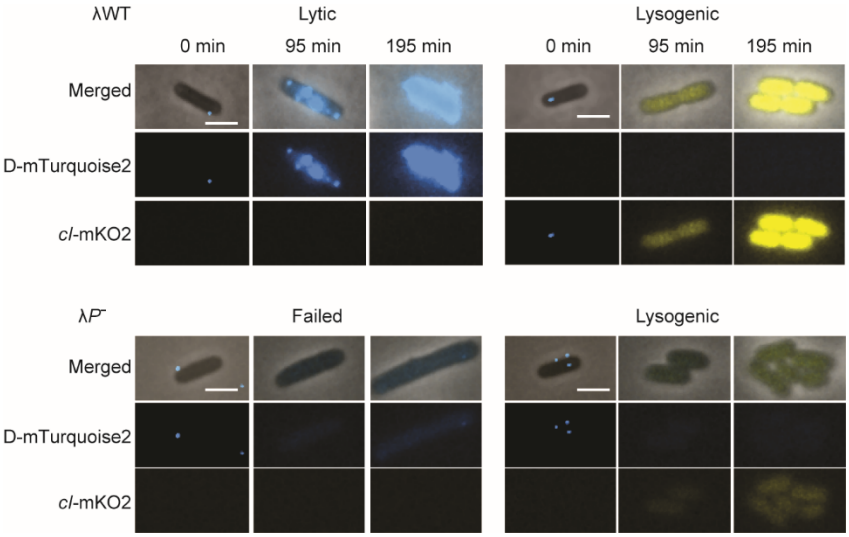

Figure S2. Representative images showing phage decision-making under the microscope. Related to Figure 1A&B.

This figure shows the same cells as in Figure 1A&B but with separate fluorescent channels. Top left: the cell is infected by one λWT phage (blue dot at 0 min), and subsequently gpD-mTurquoise2 expression (blue) is observed. Cell lysis is observed at 195 min. mKO2 expression is not detectable. Top right, the cell is infected by one λWT phage (blue dot at 0 min). *cI* reporter expression (yellow) and normal cell division are observed, indicating a successful lysogenization event. gpD-mTurquoise2 expression is not detectable. Bottom left: the cell is infected by one λ*P*- phage (blue dot at 0 min). The cell divides, and only minimal expression of gpD-mTurquoise2 is detected, indicating that phage failed to reach either the lytic or lysogenic decision. mKO2 expression is not detectable. Bottom right: the cell is infected by 3 λ*P*- phages (blue dots at 0 min). The cell divides normally, and expression of the *cI* reporter (yellow) is observed, indicating cell lysogenization. Same contrast is applied to images at 95 min and 195 min for both phages. At 0 min, a different contrast in the D-mTurquoise2 channel is applied to allow the visualization of the phage particles infecting the cell. Scale bars denote 2 μm.

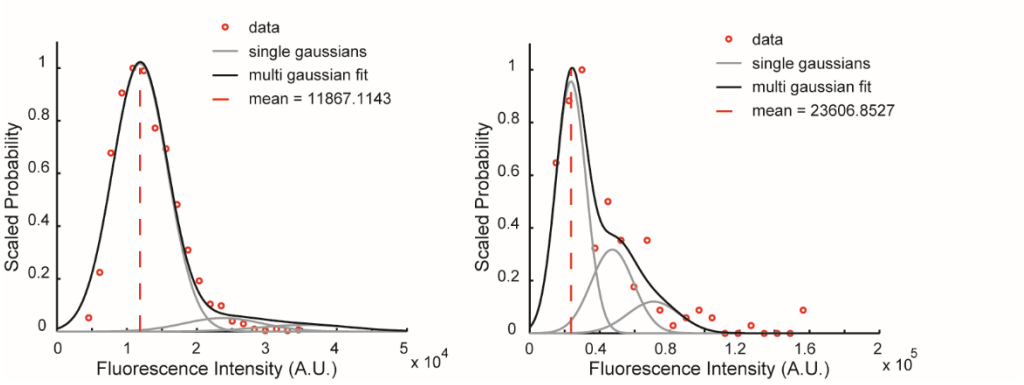

Figure S3. Calculation of single mRNA intensity for *cII*. Related to Figure 2.

(A) Calculation of the mean fluorescence intensity in the negative sample. On the x axis, fluorescence intensity is calculated as the total cell fluorescence intensity in the *cII* channel (Cy5) subtracted the background fluorescence in the non-cell area. The negative samples have a mean intensity of 11867.1143 A.U. determined by fitting to a multi-Gaussian function.

(B) Calculation of the mean fluorescence intensity in the positive sample. The fluorescence intensity of cells in the 0 min infection sample that had distinct foci were used to fit into a multi-Gaussian function, and the peak intensity was shown to be 23606.8527 A.U.. The single mRNA intensity was then approximated by subtracting 11867.1143 A.U. calculated in (A) from the 23606.8527 calculated here.

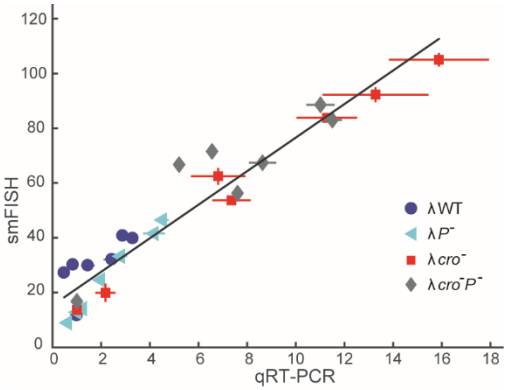

Figure S4. Comparison of average *cII* mRNA level by qRT-PCR and smFISH. Related to Figure 2.

For smFISH, only the cells with fluorescent *cII* signal were analyzed, and the average mRNA numbers at different time points for different phages were shown. For qRT-PCR, the average *cII* mRNA numbers were calculated using *ihfB* gene expression as a reference, and further normalized to the number obtained at 0 min. The correlation coefficient is 0.96, indicating a good agreement between smFISH and qRT-PCR data. Error bar denotes the standard error of the mean.

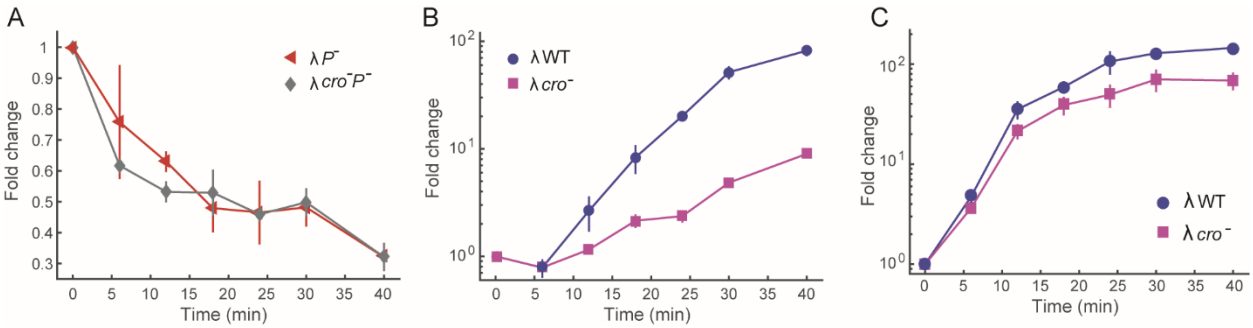

Figure S5. Phage DNA level over time detected by qPCR after infection. Related to Figure 3C.

(A) λ*P*⁻ and λ*cro*⁻*P*⁻ DNA levels over time after infection. The fold change is calculated as the ratio between phage DNA and *E. coli* DNA detected by qPCR and further normalized to the ratio at 0 min. Due to the deficiency of both phages in replication and the ongoing replication of *E. coli* DNA, the fold change drops over time after infection.

(B) λWT and λ*cro*⁻ DNA levels over time after infection. The fold change is calculated in the same way as (A). Since the phage DNA fold change shown here is also affected by *E. coli* DNA replication, we further normalized the λWT and λ*cro*⁻ numbers to the average fold change of λ*P*⁻ and λ*cro*⁻*P*⁻ calculated in (A), respectively, to obtain the relative phage DNA number increase. The results are shown in Figure 3C in the main text.

(C) λWT and λ*cro*⁻ DNA levels over time after infection at 42 ºC. As all four mutants used in this experiment carries the temperature sensitive cI_{857} allele, performing the experiment at 42 ºC abolishes the function of CI protein. Removing CI activity from the λ*cro*⁻ background does not restore the same level of DNA replication compared to λWT, suggesting that the difference in replication rate observed in (B) is not entirely due to the increased *cI* expression in λ*cro*⁻ infections.

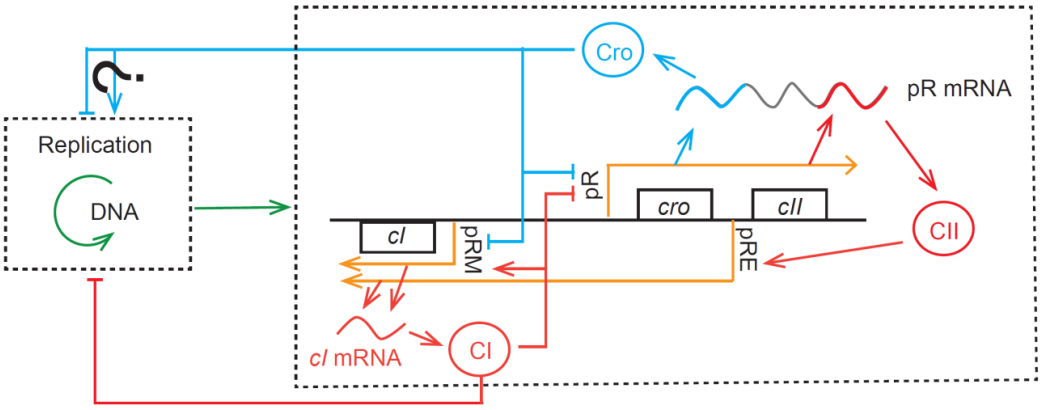

Figure S6. Model schematic of the simulated lambda decision-making network. Related to Figure 6.

The model includes DNA replication, pR and pRE transcription, and Cro, CII and CI translation. Cro represses pR transcription, yet its role in regulating DNA replication remains unknown. CII activates transcription from pRE. CI represses pR promoter and activates pRM promoter. This model is simulated stochastically using both simple and detailed approaches (see Mathematical and Computational Models section above).

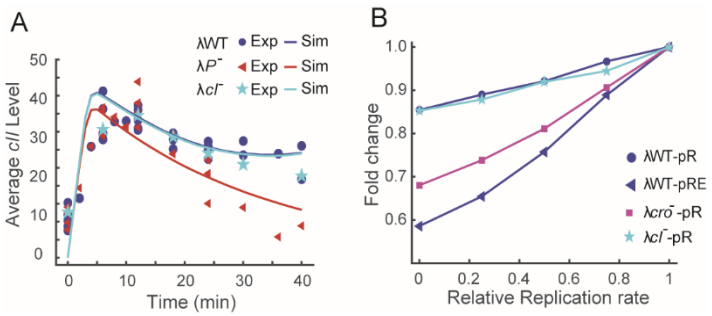

Figure S7. Detailed model performance and prediction. Related to Figure 6A-C.

(A) Prediction of the mean *cII* level from the detailed model in comparison with the experimental data. The model captures the average *cII* expression for λWT, λ*P*⁻ and λ*cI*⁻, especially in the first 24 min. Both experimental quantification and the model prediction shows that λ*cI*⁻ mutant has similar *cII* expression levels to λWT and λ*P*⁻.

(B) Prediction of the average ratio of pR and pRE mRNA levels averaged over the first 24 mins under different replication rates in different strain backgrounds from the detailed model. In the WT background, pR transcription level shows minimal changes as the replication rate varies between 0 to 1 fold of the original replication rate, whereas the pRE level varies greatly, agreeing with experimental observations. Removing Cro (λ*cro*⁻) from the model gives rise to pR transcription sensitivity to DNA replication while removing CI (λ*cI*⁻) does not cause significant changes.

Supplemental tables

Table S1. Bacterial strains used in this work. Related to Figure 1-6.

Strain Name	Relevant Genotype	Source/Reference
MG1655	sup^0	Lab collection
LE392	sup^E, sup^F	Lab collection

Table S2. Phage strains used in this work. Related to Figure 1-6.

Strain Name	Relevant Genotype	Source/Reference
λWT	λ cI_{857} *bor::Kan*^{R}	Lab collection
λ_{LZ618}	λ cI_{857} P_{am80}	Ryland Young
λP^-	λ cI_{857} P_{am80} *bor::Kan*^{R}	This work
λ_{LZ1367}	λ *D-mTurquoise2* cI_{857}*-mKO2 bor::Cm*^{R}	Lab collection
λ_{LZ1460}	λ *D-mTurquoise2* cI_{857}*-mKO2* P_{am80} *bor::Cm*^{R}	This work
λ_{LZ641}	λ *D-eyfp* cI_{857} *bor::Kan*^{R}	This work
λ_{LZ646}	λ *D-eyfp* cI_{857} P_{am80} *bor::Kan*^{R}	This work

Table S3. Plasmids used in this work. Related to Figure 1-6.

Plasmid Name	Relevant Genotype	Source/Reference
pRE-*mCherry*	*mCherry* under the control of λ pRE promoter, *Amp*^{R}	(Kobiler et al., 2005)
pBR322-pPLate**D*	gpD under the control of λ late promoter, *Amp*^{R} , for producing the mosaic λ_{LZ641} and λ_{LZ646}	(Zeng et al., 2010)
pACYC177-pPLate*D	gpD under the control of λ late promoter, *Amp*^{R}, for producing the mosaic WT and P^- phage with double reporters	Lab Collection
pBR322-*Pam80*	For recombination to make P^- phages	This work
pER157	For recombination to make *bor::Kan*^{R}	(Zhang and Young, 1999)

Table S4. Primers used in this work. Related to Figure 1-6.

Primer Name	Primer Sequence	Source/Reference
ihfB-forward	5'-ACCACGTACCGGACGTAATC	(Shao et al., 2017)
ihfB-reverse	5'-ATCGCGCAGTTCTTTACCAG	(Shao et al., 2017)
cII-forward	5'-GCAGATCAGCAGGTGGAAGA	(Shao et al., 2017)
cII-reverse	5'-AATCGAGCCATGTCGTCGTC	(Shao et al., 2017)
E-for	5'- CTGGGTGAACAACTGAACCG	This work
E-rev	5'- ATCCGTGTCATCAAGCTCCT	This work
dxs-for	5'- CGAGAAACTGGCGATCCTTA	(Lee et al., 2006)
dxs-rev	5'- CTTCATCAAGCGGTTTCACA	(Lee et al., 2006)

Table S5. Sequences of the probes for detecting the lambda *cII* mRNA. Related to Figure 2.

*cII*_1	5'-CGTTTGTTTGCACGAACCAT	*cII*_25	5'-CCACAGAAAGGTCGTTTTCT
*cII*_2	5'-TCTCGATTCGTAGAGCCTCG	*cII*_26	5'-TGAATTGCAGCATCCGGTTT
*cII*_3	5'-GCGATTTTGTTAAGCAACGC	*cII*_27	5'-ATGTCAAACATCCACTCTGC
*cII*_4	5'-TGTCTTCTCAGTTCCAAGCA	*cII*_28	5'-TGATGGTGCGATAGTCTTCA
*cII*_5	5'-GCTGATCTGCGACTTATCAA	*cII*_29	5'-CATCAGGCGGATATCGTTAG
*cII*_6	5'-AGAACTTTGGAATCCAGTCC	*cII*_30	5'-TTACCGGACCAGAAGTTGTC
*cII*_7	5'-CCCATTCAAGAACAGCAAGC	*cII*_31	5'-TCCACTTATCGCGGAGTTTG
*cII*_8	5'-AATCGAGCCATGTCGTCGTC	*cII*_32	5'-TTTGGTTTGCTGGCTGTCAC
*cII*_9	5'-AATCGCAGCAACTTGTCGCG	*cII*_33	5'-ATAGATCCACCCCGTAAATC
*cII*_10	5'-CCGGGCGTTTTTTATTGGTG	*cII*_34	5'-TCTGCTCACGGTCAAAGTTA
*cII*_11	5'-GATTTGTTCAGAACGCTCGG	*cII*_35	5'-CTTTTCGTCGTACTGTTCCG
*cII*_12	5'-AATGACCTCAGAACTCCATC	*cII*_36	5'-GAACACACCGTTGATGATCT
*cII*_13	5'-TGACTCCTGTTGATAGATCC	*cII*_37	5'-TTCGTTCTGGTCACGGTTAG
*cII*_14	5'-ATCGAGATCTGCCACATTAC	*cII*_38	5'-TTTTCCCGAAAAGCCAGAAC
*cII*_15	5'-TTGATAGTCTGGCGTAACCA	*cII*_39	5'-CGTTAACCTGTTCCATCGTG
*cII*_16	5'-GAATAAGCCTCAAGCAGCAT	*cII*_40	5'-AGAAATGGTCGATTCTGCCG
*cII*_17	5'-AACTGTCGCTTGGTCAGATC	*cII*_41	5'-ATATCAACCAGCTCGCTGAC
*cII*_18	5'-CAGAATGGCAAGCAGCACTT	*cII*_42	5'-CTTCCGGCAATACTCGTAAA
*cII*_19	5'-ATCGGTGATTCTGTCCATTG	*cII*_43	5'-AGTAGTGCGCGTTTGATTTC
*cII*_20	5'-TTGCACCGTTTGACAGGTAA	*cII*_44	5'-CTGATACAGGTTGGTAACCA
*cII*_21	5'-GACGAGTTCTAACTTGGCTT	*cII*_45	5'-GTAATTCCGCATCAGTAAGC
*cII*_22	5'-TTTTGAGGGATGCACCATTC	*cII*_46	5'-CTCACCACGGTTAATTCTCG
*cII*_23	5'-CTCGTTTTAGGGGATTTTCC	*cII*_47	5'-GTGCACGATTTAGAGGTCTA
*cII*_24	5'-ATTCGCCAGAATTCTCTGAC	*cII*_48	5'-CATACACTTGCTCCTTTCAG

Table S6. Reactions for the simple stochastic model. Related to Figure 6.

Reaction	Reaction rates ν $[X]$ denotes the concentration of X.	Description
$DNA \xrightarrow{\nu_1} DNA + RNA_{CI}$	$\nu_1 = k_{RE} \cdot \left(\frac{\kappa_{CII}[CII]^{n_{CII}}}{1+\kappa_{CII}[CII]^{n_{CII}}}\right)$	Transcription of *cI* from pRE promoter
$DNA \xrightarrow{\nu_2} DNA + RNA_{CI}$	$\nu_2 = k_{RM} \cdot \left(\frac{\kappa_{CI}[CI]^{n_{CI}}}{1+\kappa_{CI}[CI]^{n_{CI}}+\kappa_{CRO}[Cro]^{n_{Cro}}}\right)$	Transcription of *cI* from pRM promoter
$RNA_{CI} \xrightarrow{\nu_3} \phi$	$\nu_3 = d_{RNA_{CI}}$	Degradation of pR mRNA
$RNA_{CI} \xrightarrow{\nu_4} RNA_{CI} + CI$	$\nu_4 = \sigma_{CI}$	Translation of CI protein
$CI \xrightarrow{\nu_5} \phi$	$\nu_5 = d_{CI}$	Degradation of CI protein
$DNA \xrightarrow{\nu_6} DNA + pR$	$\nu_6 = k_R \cdot \left(\frac{1}{1+\kappa_{CI}[CII]^{n_{CI}}+\kappa_{CRO}[Cro]^{n_{Cro}}}\right)$	Transcription of pR mRNA from unbound pR promoter.
$pR \xrightarrow{\nu_7} \phi$	$\nu_7 = d_{pR}$	Degradation of pR mRNA
$pR \xrightarrow{\nu_8} pR + CII$	$\nu_8 = \sigma_{CII}$	Translation of CII protein
$pR \xrightarrow{\nu_9} pR + Cro$	$\nu_9 = \sigma_{Cro}$	Translation of Cro protein
$CII \xrightarrow{\nu_{10}} \phi$	$\nu_{10} = d_{CII}$	Degradation of CII protein
$Cro \xrightarrow{\nu_{11}} \phi$	$\nu_{11} = d_{Cro}$	Degradation of Cro protein
$DNA \xrightarrow{\nu_{12}} 2\ DNA$	$\nu_{12} = \begin{cases} r_0 \cdot DNA \cdot \frac{1}{1+(\kappa_{CI}^{DNA}[CI])^{n_{CI}{}^{DNA}}} \cdot \frac{1}{1+\left(\frac{t}{T}\right)^{n_T}}, & \text{if Cro is nonfunctional} \\ r_{cro} \cdot DNA \cdot \frac{1}{1+(\kappa_{CI}^{DNA}[CI])^{n_{CI}{}^{DNA}}} \cdot \frac{1}{1+\left(\frac{t}{T}\right)^{n_T}} & \text{if Cro is functional} \end{cases}$	Viral DNA replication rate

Table S7. Optimal parameters for simple stochastic model. Related to Figure 6.

Parameter description	Parameter symbol	Parameter value	Units
Transcription from pRE	k_{RE}	1.06	min^{-1}
Transcription from pRM	k_{RM}	0.128	min^{-1}
Transcription from pR	k_R	8.92	min^{-1}
CII-pRE association constant	κ_{CII}	1/172	nM
CI-pRM/R association constant	κ_{CI}	1/49	nM
Cro-pRM/R association constant	κ_{Cro}	1/23	nM
Degradation of pR transcripts	d_{pR}	0.033	min^{-1}
Degradation of CI transcripts	$d_{RNA_{CI}}$	0.119	min^{-1}
Degradation of CI proteins	d_{CI}	0.040	min^{-1}
Degradation of Cro proteins	d_{Cro}	0.018	min^{-1}
Degradation of CII proteins	d_{CII}	0.43	min^{-1}
Translation rate of CI	σ_{CI}	0.28	min^{-1}
Translation rate of CII	σ_{CII}	0.50	min^{-1}
Translation rate of Cro	σ_{Cro}	0.266	min^{-1}
Hill function sensitivity parameter for CI binding to DNA	n_{CI}	3.33	Dimensionless
Hill function sensitivity parameter for Cro binding to DNA	n_{Cro}	3.68	Dimensionless
Hill function sensitivity parameter for CII binding to DNA	n_{CII}	3.13	Dimensionless
Rate of viral DNA replication when Cro is nonfunctional	r_0	0.3	min^{-1}
Rate of viral DNA replication when Cro is functional	r_{cro}	0.16	min^{-1}
Concentration of CI at which CI causes replication rate to drop by 50%	κ_{CI}^{DNA}	23	nM
Hill function sensitivity parameter for CI's downregulation of viral replication	n_{CI}^{DNA}	4.30	Dimensionless
CI threshold for lysogeny	CI_T	21	nM
Time for the onset of DNA replication	T	3.8	mins
Parameter controlling onset of DNA replication	n_T	4	Dimensionless

Table S8. Reactions and formulas for the detailed stochastic model. Related to Figure 6.

Reaction	Reaction rates ν $[X]$ denotes the concentration of X.	Description
$\phi \overset{\nu_1}{\rightarrow} \phi + RNA_{CI}$	$\nu_1 = \alpha \cdot k_{RE} \cdot PRE(CII_4)$	Transcription of *cI* from pRE promoter
$\phi \overset{\nu_2}{\rightarrow} \phi + RNA_{CI}$	$\nu_2 = \alpha \cdot k_{RM} \cdot [OR(0, CI_2, 0) + OR(0, CI_2, CRO_2) + OR(0, CI_2, CI_2)]$	Transcription of *cI* from pRM promoter
$RNA_{CI} \overset{\nu_3}{\rightarrow} \phi$	$\nu_3 = d_{RNA_{CI}}$	Degradation of pR mRNA
$RNA_{CI} \overset{\nu_4}{\rightarrow} RNA_{CI} + CI$	$\nu_4 = \sigma_{CI}$	Translation of CI protein
$CI \overset{\nu_5}{\rightarrow} \phi$	$\nu_5 = d_{CI}$	Degradation of CI protein
$\phi \overset{\nu_6}{\rightarrow} pR$	$\nu_6 = \alpha \cdot k_R \cdot [OR(0,0,0) + OR(CRO_2, 0,0) + OR(CI_2, 0,0)]$	Transcription of pR mRNA from unbound pR promoter.
$pR \overset{\nu_7}{\rightarrow} \phi$	$\nu_7 = d_{pR}$	Degradation of pR mRNA
$pR \overset{\nu_8}{\rightarrow} pR + CII$	$\nu_8 = \sigma_{CII}$	Translation of CII protein
$pR \overset{\nu_9}{\rightarrow} pR + Cro$	$\nu_9 = \sigma_{Cro}$	Translation of Cro protein
$CII \overset{\nu_{10}}{\rightarrow} \phi$	$\nu_{10} = d_{CII}$	Degradation of CII protein
$Cro \overset{\nu_{11}}{\rightarrow} \phi$	$\nu_{11} = d_{Cro}$	Degradation of Cro protein
$DNA \overset{\nu_{12}}{\rightarrow} 2\ DNA$	$\nu_{12} = \begin{cases} r_0 \cdot DNA \cdot \dfrac{1}{1 + (\kappa_{CI}^{DNA}[CI])^{n_{CI}{}^{DNA}}}, & \text{if Cro is nonfunctional} \\ r_{cro} \cdot DNA \cdot \dfrac{1}{1 + (\kappa_{CI}^{DNA}[CI])^{n_{CI}{}^{DNA}}}, & \text{if Cro is functional} \end{cases}$	Viral DNA replication rate
$2Cro \underset{\nu_{14}}{\overset{\nu_{13}}{\rightleftarrows}} Cro_2$	$\nu_{13} = \gamma_{Cro}^{on}$ $\nu_{14} = \gamma_{Cro}^{off}$	Cro dimerization
$2CI \underset{\nu_{16}}{\overset{\nu_{15}}{\rightleftarrows}} CI_2$	$\nu_{15} = \gamma_{CI}^{on}$ $\nu_{16} = \gamma_{CI}^{off}$	CI dimerization

$2CII \underset{\nu_{18}}{\overset{\nu_{17}}{\rightleftarrows}} CII_2$	$\nu_{17} = \gamma_{CII}^{on}$ $\nu_{18} = \gamma_{CII}^{off}$	CII dimerization
$2CII_2 \underset{\nu_{20}}{\overset{\nu_{19}}{\rightleftarrows}} CII_4$	$\nu_{19} = \gamma_{CII}^{on}$ $\nu_{20} = \gamma_{CII}^{off}$	CII dimer undergoing dimerization
$CII_4 + PRE(0) \underset{\nu_{22}}{\overset{\nu_{21}}{\rightleftarrows}} PRE(CII_4)$	$\nu_{20} = \delta_{CII}^{on}$ $\nu_{21} = \delta_{CII}^{off}$	CII tetramer binding to pRE promoter
α	$\frac{1}{1 + \varepsilon DNA}$	Proportionality factor which reduced transcription rate per DNA
oR region binding reactions	Not explicitly written out, but described below in notes for Table S8	

Notes for Table S8:

The reactions and variables are similar to those in Table S7, but with some modifications that come in from the detailed model. The number of pRE promoters bound by CII tetramers is given by $\boldsymbol{PRE(CII_4)}$ and the amount not bound by CII tetramers is given by $\boldsymbol{PRE(0)}$. The notation we used in the model for the number of DNAs with a certain oR binding configuration is $\boldsymbol{OR(x, y, z)}$ where $\boldsymbol{x, y, z}$ can each assume a value of $\boldsymbol{0}$, $\boldsymbol{CI_2}$, or $\boldsymbol{Cro_2}$ to denote what is currently bound to operator site 3, 2, and 1 respectively. For example, $\boldsymbol{OR(0, CI_2, Cro_2)}$ is equal to the number of DNAs which have operator site 3 empty, operator site 2 bound by CI dimer, and operator site 1 bound by Cro dimer. The value of 0 here denotes an empty operator site. A typical reaction involving the binding of the oR region is given below:

$$\boldsymbol{Cro_2 + OR(0, 0, Cro_2) \underset{\delta_{Cro}^{off}}{\overset{\delta_{Cro}^{on}}{\rightleftarrows}} OR(0, Cro_2, Cro_2)}$$

The code for this detailed simulation is uploaded separately as Data S1.

Table S9. Optimal parameters for detailed stochastic model. Related to Figure 6.

Parameter description	Parameter symbol	Parameter value	Units
Transcription rate from pR	k_R	13.7	min^{-1}
Transcription rate from pRM	k_{RM}	0.36	min^{-1}
Transcription rate from pRE	k_{RE}	0.26	min^{-1}
Translation rate of Cro	σ_{Cro}	4.37	min^{-1}
Translation rate of CII	σ_{CII}	0.27	min^{-1}
Translation rate of CI	σ_{CI}	1.82	min^{-1}
CI dimerization on rate	γ_{CI}^{on}	0.023	min^{-1}
CI dimerization off rate	γ_{CI}^{off}	0.0036	min^{-1}
Cro dimerization on rate	γ_{Cro}^{on}	0.0016	min^{-1}
Cro dimerization off rate	γ_{Cro}^{off}	0.0076	min^{-1}
CII dimerization on rate	γ_{CII}^{on}	0.0031	min^{-1}
CII dimer off rate	γ_{CII}^{off}	0.0061	min^{-1}
CI dimer oR operator on rate	δ_{CI}^{on}	0.0057	min^{-1}
CI dimer oR operator off rate	δ_{CI}^{off}	0.015	min^{-1}
Cro dimer oR operator on rate	δ_{Cro}^{on}	0.0089	min^{-1}
Cro dimer oR operator off rate	δ_{Cro}^{off}	0.0083	min^{-1}
CII dimer DNA on binding rate	δ_{CII}^{on}	0.0107	min^{-1}
CII dimer DNA off binding rate	δ_{CII}^{off}	0.0049	min^{-1}
cI mRNA degradation rate	d_{pRE}	0.45	min^{-1}
cII mRNA degradation rate	d_{pR}	0.032	min^{-1}
Degradation rate of Cro	d_{Cro}	0.043	min^{-1}
Degradation rate of CI	d_{CI}	0.041	min^{-1}
Degradation rate of CII	d_{CII}	0.074	min^{-1}
DNA replication rate when Cro is mutated	r_0	0.155	min^{-1}
DNA replication rate when Cro is not mutated	r_{Cro}	0.2	min^{-1}
Onset of DNA replication parameter	T	5	min

Parameter controlling onset of DNA replication	n_T	0.55	Dimensionless
Threshold for lysogeny	CI_T	25	Dimensionless
Parameter controlling DNA-copy number dependence on transcription rate per gene	ε	0.037	Dimensionless

Transparent methods

Plasmid, bacterial and phage strains

The λP^- phage (λ cI_{857} P_{am80} *bor::Kan*^{R}) was constructed using protocols as previously described (Shao et al., 2015) by recombining the parental strain (λ cI_{857} P_{am80}, gift of Ryland Young) with plasmid pER157 (Zhang and Young, 1999) to replace the nonessential *bor* gene region with a Kanamycin resistance cassette. The fluorescent λP^- phage bearing double reporters, λ_{LZ1460}, was constructed by crossing the WT phage λ_{LZ1367} (Trinh et al., 2017) with plasmid pBR322-P_{am80}. This plasmid carries a fragment of the lambda genome which covers part of the *P* gene, with the CAG encoding Q at the 69 AA position mutated to an amber stop codon TAG, corresponding to the P_{am80} mutation. λ_{LZ1367} was titered on LE392 carrying plasmid pBR322-P_{am80} to produce confluent plates with connecting plaques. The phages collected from this plate were then used to screen for the recombinant strain λ*D-mTurquoise2* cI_{857}*-mKO2* P^- *bor::Kan*^{R} (λ_{LZ1460}). The amber mutation in the *P* gene allows the phages to propagate on suppressor strain LE392 but not on non-suppressor strain MG1655. Therefore, a mixture of LE392 and MG1655 cells at exponential phase was used for titering and the phages that form turbid plaques were then selected and further confirmed by sequencing.

The EYFP labeled fluorescent WT phage (λ_{LZ641}) was obtained by crossing phage λeyfp (λcI_{857} *D-eyfp Sam7*) (Alvarez et al., 2007) with a plasmid pER157 (Zhang and Young, 1999), which contains WT *S* gene and *bor::Kan*^{R}*.* The resulting lysate was then screened for the ability to grow on Kanamycin plates after lysogenization on the non-suppressor strain, MG1655. The resulting lysogens were then further tested for the ability to lyse after induction, resulting in phage λ_{LZ641} (λcI_{857} *D-eyfp bor::Kan*^{R})*.* The EYFP labeled λP^- phage (λ_{LZ646}) was obtained by crossing phage λ_{LZ641} with another phage (λ cI_{857} P^- *bor::Kan*^{R}), and screened for smaller plaques on LE392, as fluorescently labeled phages are unstable and usually form smaller plaques compared to non-fluorescent phages. This phage strain was confirmed as P^- by its inability to form plaques on MG1655 and by sequencing.

As fluorescently labeled phages are unstable, we transformed plasmid pLate*D into the lysogens before induction, to create stable mosaic phages containing a mixture of wild type gpD (from the plasmid) and gpD-EYFP (from the phage genome). The phages were then purified following protocols described in (Zeng et al., 2010) and used for live-cell imaging. Specifically, lysogenic cells were diluted from an overnight culture into 500ml of LBM (LB + 10 mM $MgSO_4$) and grown at 30 °C to OD = 0.6 with mild shaking at 180 rpm. The lysogens were then induced in a 42 °C water bath with shaking for 20 min and then transferred to a 37 °C shaker. Culture

lysis typically occurs within 1 hr of induction and the resulting lysate was treated with 2% $CHCl_3$, and then centrifuged to remove cell debris and chloroform. The phage lysate was next treated with 1 µg/ml of DNase and RNase, and precipitated with 10% wt/vol PEG8000 and 1M NaCl. The phage/PEG precipitant was then resuspended in SM buffer. After that, $CHCl_3$ was used to partition the PEG from the phages. This concentrated phage lysate (5-10 ml) was ultracentrifuged using a CsCl step gradient, extracted, and subjected to CsCl equilibrium centrifugation. The band corresponding to lambda phages were then extracted, and the lysate was then dialyzed in SM buffer prior to use in subsequent experiments.

The bacterial, phage strains, plasmids and primers are listed in Table S1, S2, S3, and S4, respectively.

RNA smFISH

We used *cI* probes reported in ((Zong et al., 2010), ordered pre-labeled with TAMRA from Biosearch Technologies. pR (*cII*) probes are designed (the sequences can be found in Table S5), synthesized and labeled with Cy5 (GE Healthcare Life Sciences, #PA15000) following protocols described (Skinner et al., 2013). Briefly, we pooled 7.5 µl of each of the oligo solutions (48 oligo in total for pR, 100 µM each) and added 40 µl of 1 M sodium bicarbonate, pH 8.5. We then added dye solution (1 mg of Cy5 dissolved in 2.5 µl of DMSO and 25 µl of 0.1 M sodium bicarbonate, pH 9.0) to the oligo mixture, incubated it in the dark, overnight at 37 ^{o}C. The next day, we mixed 47 µl of 3 M sodium acetate, pH 5.2, into the solution, and then added 1180 µl of 100% ethanol and incubated the sample -80 ^{o}C for 3 hr to precipitate the oligos. The oligos were then spun down and washed twice more by dissolving the pellet in 45 µl of DEPC-treated water, 5 µl of 3 M sodium acetate, pH 5.2, and 125 µl of 100% ethanol. After the washing steps, the probes were resuspended in 250 µl of 1× TE resulting in a 10× probe stock solution. The probe solution was diluted with 1× TE to make the 1× probe solution upon usage, and the labelling efficiency of the probes was determined using the NanoDrop to be 99%.

To detect the mRNA level after infection, non-suppressor strain MG1655 was used as the host for infection. The overnight culture MG1655 was diluted 1:1000 into fresh LBMM (LB supplemented with 0.2% maltose and 10 mM $MgSO_4$) and grown at 37 ^{o}C with shaking at 265 rpm until OD_{600} ~0.4. The cells were then collected by centrifugation at 2000 ×g for 15 min and re-suspended in 1/10 volume of pre-chilled LBMM. For each sample to be collected, 1 ml of concentrated cells were used for infection. An appropriate amount of phages was added to reach an API of 0.1-0.2 and mixed well. For the negative control, we added the same volume of

SM buffer (phage buffer, 100 mM NaCl, 10 mM $MgSO_4$, 0.01% gelatin, 50 mM Tris-Cl, pH 7.5) to the sample. We incubated the samples on ice for 30 min to allow phage adsorption, then transferred the samples to a 35 ^oC water bath for 5 min to allow phage DNA ejection. After this step, we transferred 750 µl of each sample to 7 ml of pre-warmed LBGM (LB supplemented with 0.2% glucose and 10 mM $MgSO_4$) and incubated it in a 30 ^oC water bath with mild shaking at 225 rpm. As all our phage strains except for λ*cI*$^-$ carry the temperature sensitive cI_{857} allele, whose gene product is unstable at 37 ^oC or above, this infection step is performed at 30 ^oC for all our experiments unless otherwise stated. At each time point, we poured the sample into a 50 ml tube with 860 µl of 37% formaldehyde (final concentration 3.7%) for quick fixation, and incubated the mixture for 30 min at room temperature on a nutator. The samples were then treated following protocols described (Skinner et al., 2013). Briefly, after fixation, each sample was washed three times with 1× PBS to remove excess formaldehyde. The cells were then permeabilized in 70% ethanol for 1 hr at room temperature and spun down subsequently. The cell pellet was resuspended in wash solution (40% (wt/vol) formamide, 2× SSC) and incubated at room temperature for 5 min and spun down again. For hybridization, the cells were resuspended in 25 µl of hybridization solution (40%(wt/vol) formamide, 2× SSC, 1 mg/ml *E. coli* tRNA, 2 mM ribonucleoside-vanadyl complex and 0.2 mg/ml BSA) with each probe at a final concentration of 1 µM. Samples were then incubated in a 30 ^oC water bath for overnight. Following that, samples were washed three times by incubating the cells in wash solution for 30 min in a 30 ^oC water bath. After the third repeat of washing, 10 µg/ml DAPI was added to the wash solution to stain the *E. coli* and phage DNA. Cells were resuspended in 2× SSC and imaged immediately. The detailed microscopy settings can be found in the **Microscopy** section.

qPCR for quantifying phage DNA and RNA levels

Phage infections were set up following the same procedure as for RNA smFISH but with 0.5× volume. At each time point, samples were taken and prepared for qRT-PCR to detect the *cI* and *cII* mRNA levels following our previously established protocols (Shao et al., 2017). Briefly, at each time point, samples were immediately poured into 5 ml ice-cold methanol. Samples were then spun down at 4000×*g* for 4 minutes, at 4 ^oC. The cell pellet was resuspended in 1 ml of RNA protect Bacteria Reagent (Qiagen, 76506), followed by incubation for 5 minutes at room temperature. Afterwards, the cells were spun down at 5000×*g* for 5 minutes at room temperature. After discarding the supernatant, the cells were kept at -20 ^oC until all samples were collected. RNA extraction was done using the RNeasy Mini Kit (Qiagen, 74104), followed by DNA digestion with the TURBO DNA-free kit (Ambion, AM1907) for a total of 80 minutes. Reverse transcription

was then performed using the High Capacity RNA-to-cDNA kit (Applied Biosystems, 4387406). The resulting cDNA was then quantified using the SYBR Green PCR master mix. The *ihfB* mRNA was used as a reference gene to allow the comparison of *cI* and *cII* mRNA levels over time. To detect the phage DNA number, the samples were taken following the similar procedures as for qRT-PCR. After the cold-methanol step, the samples were frozen and we extracted DNA at this step using the UltraClean Microbial DNA Isolation Kit (MO BIO Laboratories, #12224-50). The DNAs were then diluted and used for qPCR using primers targeting the phage genome. The *E. coli* DNA number was used as a reference using primers targeting the *dxs* gene (Lee et al., 2006).

Microscopy

To image the smFISH samples, after the suspension of the cells in 2×SSC, 1 µl of the sample is placed on a cover slip and topped with a piece of 1.5% agarose pad (prepared with 1×PBS). The sample was then imaged immediately on an inverted microscope (Ti-E, Nikon, Tokyo, Japan). Images were taken using 100× objective (Plan Fluo, NA 1.40, oil immersion) with standard filter sets and a cooled EMCCD camera (iXon 3 897, Andor, Belfast, United Kingdom). A series of 5 z-stack images with spacing of 300 nm in the Cy5 (for *cII*, 200 ms exposure, Cy5 filter, Nikon 96366), and TAMRA (for *cI*, 200 ms exposure, Cy3 filter, Nikon 96323) channels were taken, while one image was taken at the focal plan for the phase contrast (100 ms exposure) and DAPI (30 ms exposure, DAPI filter, Nikon 96310) channels.

The real-time live-cell imaging of the double reporter λWT and λP^- phage infection are performed as described (Trinh et al., 2017). Briefly, overnight MG1655 cells grown in M9M (M9 supplemented with 0.4% maltose) were diluted 1:100 into fresh M9M medium and grown to OD_{600}~0.4. The cells were then harvested and concentrated by 10 fold by resuspending in 1/10 volume of M9M. The cells were then infected with phages at different APIs, following an incubation on ice for 30 min, and 5 min in a 35 ^oC water bath. The cells were then diluted and placed on a coverslip, and topped with 1.5% agarose pad made with M9M. To observe the phages infecting each cell at the beginning of the infection, a series of 9 z-stack images with spacing of 300 nm in the mTurquoise2 channel (200 ms exposure, CFP filter, Nikon 96361) were taken, while images were also taken at the focal plane in the phase contrast (100 ms exposure) and the mKO_2 channel (100 ms exposure, custom filter, Chroma 49309). After that, time-lapse movies were set up without z-stacks to track the progression of phage infection by imaging every 5 min in the phase contrast (100 ms exposure), mTurquoise2 (40 ms exposure) and mKO_2 (100 ms exposure) channels, for a total length of 4 hrs.

The real-time live-cell imaging of the EYFP labeled λWT and λ*P*⁻ phages were done following protocols as described in (Zeng and Golding, 2011). Briefly, overnight MG1655[pRE-*mCherry*] cells grown in LBMM were diluted 1:1000 into fresh LBMM medium until OD_{600}~0.4. The cells were then harvested by centrifugation and resuspended in 1/10 volume of fresh LBMM. The infections were done following the same protocols, and the samples were imaged using a 1.5% agarose pad made with LBM (LB supplemented with 10 mM $MgSO_4$) (Zeng and Golding, 2011). To observe the phages infecting each cell at the beginning of the infection, a series of 9 z-stack images with spacing of 300 nm in the YFP (400 ms exposure, YFP filter, Nikon 96363) were taken, while images were also taken at the focal plane in the phase contrast (100 ms exposure) and the mCherry channel (100 ms exposure, TexasRed filter, Nikon 96365). After that, time-lapse movies were set up to track the progression of phage infection by taking images every 5 min in the phase contrast (100 ms exposure), YFP (100 ms exposure) and mCherry (100 ms exposure) channels, for a total length of 4 hrs.

mRNA number quantification

Microscope images were first processed using Schnitzcells, which recognizes and segments individual cells. The total cell fluorescence intensity was calculated by summing the intensities within the cell boundaries and subtracting the background fluorescence. The average intensity of the cell was calculated by dividing the total intensity by the cell size. At 0 min after infection, a small subpopulation of cells displayed a low level of *cII* mRNA expression, typically as a single focus, distinct from the negative samples, which lack phage infection. Because *cII* mRNA forms clusters under our experimental conditions, those single foci may correspond to either a single mRNA or multiple mRNAs clustered together. The total fluorescence intensities of those cells and the cells from the negative samples were fitted into multi-Gaussian functions (Figure S3), and the differences between them are designated as the intensity for a single *cII* mRNA. The same calculation method was applied to calculate the single mRNA intensity of *cI*, where the cells with low expression of *cI*, typically at 6 min, were used. Once the single mRNA intensity was obtained, the number of mRNA in each cell was calculated by (T-m*S)/A, where T is the total intensity of the cell, m is the median of the average intensity of the cells from the negative sample, S is the size of the cell, and A is the intensity of one mRNA calculated as described above.

Mathematical and Computational Models

To understand why *cII* mRNA expression is insensitive to DNA replication, we developed two models at different levels of detail. The major difference between the two models is in how the regulation of transcription was modeled. In the simple model, we assumed that the total regulation of viral promoters by transcription factor levels could be described by a general Hill function with Hill-parameters determined by fitting to the data. Alternatively, in the detailed model we explicitly simulated the on and off binding of transcription factors to the operator sites of the viral promoters to regulate transcription. Both modeling approaches led to consistent results, and are described in the following sections.

The Simple Stochastic Model

Results from this model are shown in the main text. The model uses Hill functions to describe the response of promoters to the transcription factors instead of explicitly simulating the on/off binding of transcription factors, and it is therefore referred to as the simple model. The model schematic is shown in Figure S6, the reactions are summarized in Table S6 and the rate constants are summarized in Table S7.Overall, our model is heavily based on prior models of the phage lambda gene regulatory network (Joh and Weitz, 2011; Robb and Shahrezaei, 2014; Weitz et al., 2008), and is most similar to the model in (Cortes et al., 2017). This model is simulated using the Gillespie Algorithm (Gillespie, 1976, 2007). To avoid repeating the details of other works, the reader is directed to the relevant references where these modeling approaches were more explicitly described. Nevertheless, we discuss the major features of the model below.

Transcription reactions

The general form of transcription reactions is as follows:

$$\text{transcription rate} = k \cdot \alpha \cdot D$$

Where D is the number of the transcribing promoters (equal to the number of DNA molecules since we have 1 promoter of each type per DNA molecule), α describes the activity of the promoters, and k is a proportionality constant. Next, we will describe the transcription of various mRNAs in more detail.

cI mRNA is transcribed from both the pRE and pRM promoters. Transcription of *cI* mRNA from the pRE promoter depends on the promoter being activated by CII. Thus, we take the activation α_{pRE} of pRE to be a Hill function which increases from 0 to 1 as the concentration of CII

increases. Essentially, we are phenomenologically modeling CII activation of pRE according to the following equation:

$$\alpha_{pRE} = \frac{\kappa_{CII}[CII]^{n_{CII}}}{1 + \kappa_{CII}[CII]^{n_{CII}}}$$

Where [·] denotes the level of CII. The variables κ_{CII} and n_{CII} parameterize this function and were determined by fitting to experimental data. The proportionality constant from the general form of transcription reactions here is k_{RE}. Thus, the final reaction rate describing transcription of *cI* mRNA from pRE is $k_{RE}\alpha_{pRE}D$. The major advantage of this phenomenological approach is that it makes few assumptions about the underlying mechanistic details while still capturing the general behavior of transcription from this promoter.

cI mRNA can also be expressed from promoter pRM which is regulated by both CI and Cro. There are 3 operator sites located between the pRM and pR promoters. CI and Cro dimers are known to compete and bind to these operators to regulate the transcriptional activity of both pRM and pR. Depending on the binding configuration of CI and Cro, pRM will either be repressed or activated, similarly for pR. This turns out to be consistent with recent published models (Cortes et al., 2017; Joh and Weitz, 2011; Robb and Shahrezaei, 2014; Weitz et al., 2008), which treat the operator region as one single binding site to which CI and Cro competitively bind. This results in a mixed-Hill function formula which describes the activity of the pRM and pR promoters. The formula we use for the activation of pRM is:

$$\alpha_{pRM} = \frac{\kappa_{CI}[CI]^{n_{CI}}}{1 + \kappa_{CI}[CI]^{n_{CI}} + \kappa_{Cro}[Cro]^{n_{Cro}}}$$

This formula captures the fact that *cI* transcription increases as the concentration of CI increases and decreases as Cro concentration decreases. The variables $n_{CI}, n_{Cro}, \kappa_{CI}, \kappa_{Cro}$ parameterize the activation function and are determined by fitting to experimental data. At very high CI levels, expression from pRM actually drops because CI binds to the oR3 operator and blocks RNA polymerase from pRM. This feature is neglected in this simple model, but it is present in the more detailed model presented later on.

cII mRNA is transcribed from the pR promoter when pR is not bound by Cro or CI. Therefore, the activation/repression factor for *cII* transcription is:

$$\alpha_{pR} = \frac{1}{1 + \kappa_{CI}[CI]^{n_{CI}} + \kappa_{Cro}[Cro]^{n_{Cro}}}$$

This formula captures the fact that high concentrations of either CI or Cro (or both) will lead to decrease of pR transcription activity.

In this model there are 3 important Hill coefficients, namely, n_{CII}, n_{CI}, and n_{Cro}, which determine the response of transcription rates to the concentrations of viral transcription factors CII, CI, and Cro, respectively. Initial parameter optimizations of this model lead to arbitrarily high Hill coefficients when fitting to the experimental data (e.g. the value of n_{Cro} returned from the optimization protocol can be as high as 7). This was likely due to the fact that the insensitivity of *cII* mRNA levels to viral replication are strongly determined by the magnitude of the Hill coefficients, since the Hill coefficient n_{Cro} controls the strength of Cro repression. As arbitrarily large Hill coefficients are unrealistic, we constrained the Hill coefficients to have a maximum possible value of 4 during the parameter optimization. The reason for choosing a maximum value of 4 is given below.

Consider the general case of a transcription-factor X (of concentration x) which forms an n-multimer (of concentration x_n) to bind the operator region of a promoter. The dynamics which govern this system is described by the following set of equations:

$$\dot{x} = -\gamma_{on} x^n + \gamma_{off} x_n$$

$$\dot{x_n} = \gamma_{on} x^n - \gamma_{off} x_n - \delta_{on} x_n D_0 + \delta_{off} D_x$$

$$\dot{D_0} = -\delta_{on} x_n D_0 + \delta_{off} D_x$$

$$\dot{D_x} = \delta_{on} x_n D_0 - \delta_{off} D_x$$

The variables D_0 and D_x denote the unbound and bound states of the promoter. The rate constants γ_{on} and γ_{off} describe the on/off multimerization rates of X, and the constants δ_{on} and δ_{off} describe the on/off DNA-transcription factor binding rates. Since these reactions equilibrate on the order of seconds and transcription occurs on the timescale of several minutes, we can examine this system at steady state. Thus, we set all derivatives to 0 and solve for the fraction of DNA in the bound state given by $f_x = D_x/(D_x + D_0)$.

$$f_x = \frac{D_x}{D_0 + D_x} = \frac{\frac{\delta_{on}\gamma_{on}}{\delta_{off}\gamma_{off}} x^n}{1 + \frac{\delta_{on}\gamma_{on}}{\delta_{off}\gamma_{off}} x^n} \quad (1)$$

The fraction of promoter in the unbound state is simply given by $1 - f_x$:

$$(1 - f_x) = \frac{1}{1 + \frac{\delta_{on}\gamma_{on}}{\delta_{off}\gamma_{off}} x^n} \tag{2}$$

In the case of pRE, we know that in equation 1 the value of $n = 4$ since CII forms a tetramer. Past models have simulated CII as forming both dimers and tetramers, and showed that activity of pRE in the concentration of CII can be described by a Hill function with a Hill coefficient of 2 or 4 (Hoopes and McClure, 1985; Jain et al., 2005; Robb and Shahrezaei, 2014; Weitz et al., 2008). Therefore we constrained the Hill coefficient of pRE-CII to be $2 \leq n \leq 4$

In the case of transcription from pR, the binding of CI and Cro is complicated. If we first focus on only Cro binding to oR1, then the fraction of oR1 in the unbound state is given by equation (2) with $n = 2$ since Cro forms dimers. Similarly, the fraction of oR2 in the unbound state would also be given by equation (2) with $n = 2$. Thus, the total fraction of DNA which has both oR2 and oR1 in the unbound state is given by $(1 - f_x)^2$ which is the product of the probabilities of both sites being unbound:

$$(1 - f_x)^2 = \frac{1}{\left(1 + \frac{\delta_{on}\gamma_{on}}{\delta_{off}\gamma_{off}} x^2\right)^2} = \frac{1}{1 + 2\frac{\delta_{on}\gamma_{on}}{\delta_{off}\gamma_{off}} x^2 + \left(\frac{\delta_{on}\gamma_{on}}{\delta_{off}\gamma_{off}}\right)^2 x^4} \tag{3}$$

We can set $L^2 = \delta_{off}\gamma_{off}/\delta_{on}\gamma_{on}$ and rewrite this expression as:

$$\frac{1}{1 + 2\frac{\delta_{on}\gamma_{on}}{\delta_{off}\gamma_{off}} x^2 + \left(\frac{\delta_{on}\gamma_{on}}{\delta_{off}\gamma_{off}}\right)^2 x^4} = \frac{1}{1 + 2\left(\frac{x}{L}\right)^2 + \left(\frac{x}{L}\right)^4} \tag{4}$$

If the concentration of Cro is very large, then $x \gg L$, which means the factor $(x/L)^{-2} \approx 0$ and therefore:

For high Cro levels

$$(1 - f_x)^2 = \frac{1}{1+2\left(\frac{x}{L}\right)^2+\left(\frac{x}{L}\right)^4} = \frac{1}{1+\left(\frac{x}{L}\right)^4\left[2\left(\frac{x}{L}\right)^{-2}+1\right]} \approx \frac{1}{1+\left(\frac{x}{L}\right)^4} \tag{5}$$

If the concentration of Cro is low, then $x \ll L$ which means the factor $(x/L)^4 \approx 0$ and therefore:

For low Cro levels

$$(1 - f_x)^2 = \frac{1}{1+2\left(\frac{x}{L}\right)^2+\left(\frac{x}{L}\right)^4} \approx \frac{1}{1+2\left(\frac{x}{L}\right)^2} = \frac{1}{1+\left(\frac{x}{L/\sqrt{2}}\right)^2} \tag{6}$$

Since pR transcription happens when both oR1 and oR2 are unoccupied, the overall response of pR transcription to Cro concentration can be described as being proportional to $(1 - f_x)^2$ which is a decreasing Hill function. In the case of low Cro levels the Hill coefficient is approximately 2 (see equation 6), and in the case of high Cro levels the Hill coefficient is approximately 4 (see equation 5). Therefore, we searched the n_{Cro} parameter between 2 and 4 during the optimization procedure when fitting to experimental data.

Since CI also binds as a dimer to the same operator sites, we also assumed the n_{CI} parameter to be between 2 and 4. CI dimers binding to adjacent operator sites actually do have some cooperativity, so the expected value of n_{CI} would be larger than n_{Cro}, but to keep things simple we simply searched both n_{CI} and n_{Cro} between the values 2 and 4. Overall, we showed that this range allows our model to reproduce the data.

DNA replication reactions

Our experimental data showed that DNA replication is exponential, and also showed that when Cro is functional (λWT) the replication rate is higher compared to when Cro is nonfunctional (λ*cro*$^-$) (Figure 3C). The mechanism behind this phenomenon is not fully understood, and we do not attempt to model it explicitly. Therefore, the replication rate constant r in our model takes on two unique values, r_{cro} and r_0, for λWT and λ*cro*$^-$, respectively. Note that $r_{cro} > r_0$ to be consistent with experimental observations. In cases of high CI concentration (i.e., during lysogenic development), phage DNA replication stops. To capture this phenomenon, we assume the total replication reaction rate to be:

$$\text{DNA replication rate} = \begin{cases} r_0 \cdot D \cdot \dfrac{1}{1 + (\kappa_{CI}^{DNA}[CI])^{n_{DNA}}}, & \text{if Cro is nonfunctional} \\ r_{cro} \cdot D \cdot \dfrac{1}{1 + (\kappa_{CI}^{DNA}[CI])^{n_{DNA}}}, & \text{if Cro is functional} \end{cases}$$

The parameters $r_0, r_{cro}, n_{DNA}, \kappa_{CI}^{DNA}$ parameterize viral DNA replication and are determined by fitting to experimental data.

We also noted that DNA replication does not occur immediately after infection, but only begins after about 5 mins post-infection. We included this in the model as well by assuming the onset of DNA replication occurs at a time $T \leq 5$ mins which was fit to the experimental data during the optimization procedure. More specifically, we modeled the onset of DNA replication by allowing the DNA replication rate constant to increase from 0 up to its maximum value according to the following Hill function.

$$r_0 = \frac{1}{1 + \left(\frac{t}{T}\right)^{n_T}}$$

$$r_{cro} = \frac{1}{1 + \left(\frac{t}{T}\right)^{n_T}}$$

This was also done for the detailed model.

Translation reactions

Translation of CI, Cro, and CII proteins are modeled as being proportional to the total amount of their respective transcripts. For protein X, the translation rate is given by $\sigma_X \cdot m_X$ where σ_X is the translation rate per unit time and m_X is the number of mRNAs which can produce X.

Degradation reactions

All mRNAs and proteins degrade with reaction rates being proportional to their total amount. For molecule X, the degradation rate is given by $d_X \cdot N_X$ where d_X is the degradation rate of X per unit time and N_X is the number of X molecules. This applies to all RNAs and proteins, but not to DNA. We assume that DNAs are stable and cannot be degraded.

Lysogenic decisions

We have another parameter called CI_T which is defined as the threshold concentration for CI above which the simulation is marked as lysogenic. Otherwise, if CI levels remain below this threshold during the entire simulation we mark the decision outcome as lysis. This parameter was determined by fitting to a 30% probability of lysogeny at MOI = 1.

The Detailed Stochastic Model

Model assumptions

The reactions in the detailed model were identical to those in the simpler model except we removed the Hill functions and instead explicitly simulated i) CI and Cro dimers binding to the three oR operator sites (oR1, oR2, and oR3) to regulate pRM and pR transcription and ii) CII tetramers binding to the pRE promoter to activate pRE transcription. Thus, this model did not use Hill functions to describe transcriptional responses to transcription-factor levels. Specifically, we modeled CI and Cro dimerization, as well as the on/off binding of CI and Cro dimers to each of the 3 operator sites in the oR region. This binding complexity leads to a model with a total of 130 reactions (The major reactions and parameters can be found in Table S8 and S9,

respectively). In theory, the rate constant for each reaction is unique since the affinities of CI and Cro to each of the oR operator sites are unique and depend on the current bound state of adjacent operator sites. This implies that the total number of free parameters in this system could reach 130. To reduce the number of free parameters, we assumed the binding rates between DNA and CI/Cro dimers to be the same, and we did the same for the unbinding rates. This results in a model with 29 free parameters which we determined by fitting to the data. While some of these parameters have been estimated in the literature, we noted that model parameters can change when experimental conditions change. Therefore, recalibration of model parameters is necessary and we perform such a calibration using an optimization protocol (discussed later on).

In the detailed model, we also assumed that i) pR transcription is 0 when CI or Cro dimers are bound to either oR2 or oR1 ii) pRM transcription occurs only if oR3 is free and oR2 is bound by CI dimer iii) DNA replication stops if oR1 and oR2 are bound by CI dimers (which would promote DNA looping to block DNA replication as occurs in the lysogenic pathway).

Initial simulations of this detailed molecular model reproduced the *cII* mRNA data at early time points (0 - 24 mins which is the decision time window) very well. Moreover, we confirmed that Cro, but not CI, is required for the *cII* expression robustness to DNA replication by making computational mutants of Cro and CI.

While we focused on the decision time window to examine the effects of DNA replication on gene expression, we extended our simulation for longer to check the expression of *cII* at later time points, and some interesting phenomena were observed. Under the model assumptions, we find that, at 30 min and 40 min, the predicted *cII* mRNA level increases drastically while experiments showed that *cII* mRNA level remain almost constant at the late time points (Figure 3A).

In the simulation, we treated every copy of DNA equally and expression from every DNA is possible, but in reality, some DNA at the late stage might not be able to express genes. In the early stage, DNA replication happens in the theta mode, which produces circular DNA. Later, replication switches into sigma mode, where long concatemeric DNAs are produced, and those DNAs are later packaged into phage capsids to produce phage progeny. We do not know whether the form of DNA (circular vs linear, concatemeric DNA) would be expressed the same. Moreover, at the later time points, some DNAs start to be packaged into phage capsids, and this process can also reduce the effective transcription rate per DNA.

Alternatively, it is possible that when DNA copy counts are high, host resources required for gene expression might be limited, therefore causing the effective transcription rate to decrease. In fact, it has been reported that the transcription rate per DNA drops when high copies of exogenous gene circuits are introduced into the cells simply because there are limited requisite host factors available (Qian et al., 2017; Shopera et al., 2017). Specifically for phage lambda, past work has demonstrated that phage infections reduce host cell transcription and translation (Howes, 1965; Liu et al., 2013; Terzi and Levinthal, 1967).

In summary, we believe that at the late stage of phage infection, transcription rate per DNA is likely to change due to various factors discussed, and the lack of those factors in our model can lead to the increased *cII* expression level that was predicted at late time points.

Detailed model with modified transcription rate

To account for the aforementioned factors that can affect gene expression at the late stage of infection, we assumed that the baseline transcription rates (e.g. transcription rate per promoter) were inversely proportional to the number of phage DNA (a detailed derivation of this relationship can be found in the following section). Specifically, we multiplied the original transcription rates by a factor $1/(1+\varepsilon D)$. For example, if the transcription rate per gene is k_0, then the modified (effective) transcription rate k_{eff} per DNA is calculated as follows:

$$k_{eff} = \frac{k_0}{1+\varepsilon D} \tag{7}$$

Here, ε is a constant and $\varepsilon > 0$ such that overall transcription per DNA is down regulated as D increases. Note that this modification (equation 7) is consistent with either of our hypothesized reasons previously described, namely that either i) late DNAs are not transcribable or ii) there is competition for host-factors required for transcription initiation.

Including this modification of transcription rate allows the model predictions to match the experimental measurements better, especially for *cII* expression at 30 and 40 min (Figure S7A). Based on this new modified model, we examined the dependence of *cII* expression robustness on Cro and CI by removing them one at a time from the simulation. We observed the same phenomenon as in the existing model, and show that removing Cro abrogates the *cII* expression robustness (Figure S7B).

Derivation of the dependence of transcription rate on DNA copy number when host resource is limited

To examine how effective transcription rates per promoter can be affected by DNA copy numbers, we compared two simple models of transcription. The first model (model A, equations 1A and 2A) simulates transcription occurring without the requirement of host factors, whereas the second model (model B, equations 3B – 5B) simulates transcription occurring only after a host transcription-factor binds to the promoter region.

Model A (no requirement for host transcription factors)		Model B (transcription requires host factors)	
$D \xrightarrow{k_0} D + x$	1A	$T_0 + D_0 \underset{\gamma_{off}}{\overset{\gamma_{on}}{\rightleftarrows}} D_T$	1B
$x \xrightarrow{d_x} \phi$	2A	$D_T \xrightarrow{k_0} D_T + x$	2B
		$x \xrightarrow{d_x} \phi$	3B

In model A, D is the total DNA copy count, x is the mRNA of gene X, k_0 is the transcription rate per promoter, and d_x is the degradation rate of the mRNA. The rate-law describing the dynamics of mRNA for model A is given by:

$$\dot{x} = k_0 D - d_x x \tag{8}$$

Thus, the transcription rate per DNA for model A is k_0.

In model B, D is again the total DNA copy count, D_0 is the number of DNAs not bound by host-factor, and D_T is the number of DNAs bound by host-factor (thus $D = D_0 + D_T$). Similarly, the variable T is the total number of host-factors in the cell, T_0 is the number of host-factors in the unbound state, and T_E is the number of host-factors bound to the promoter regions of all other transcribable genes on the host's genome and viral DNAs (thus $T = T_0 + D_T + T_E$). Since the number of other transcribable genes (not including gene X) in the cell is high, we expect the fraction $\delta = T_E/T$ to be relatively large.

For model B, the constants γ_{on} and γ_{off} are the host-factor on/off binding rates for the DNA promoter region. The constant k_0 is the transcription rate per host-factor-bound DNA, and d_x is the degradation rate of the mRNA. The rate-law describing the dynamics of mRNA for model B is given by:

$$\dot{x} = k_0 D_T - d_x x \tag{9}$$

We can rewrite this in terms of the total DNA copy count D by writing:

$$D_T = \left(\frac{D_T}{D}\right) \cdot D = f_T \cdot D$$

Here f_T is just fraction of DNA promoters bound by host factors. We then plug this expression into equation 9 to get equation 10.

$$\dot{x} = k_0 f_T D - d_x x \tag{10}$$

Thus, the new effective transcription rate per DNA promoter for model B is given by $k_{eff} = k_0 f_T$. In order to compare the transcription rate per DNA promoter for model A and B, we first calculated f_T.

Since protein-DNA binding is fast (on the order of seconds) compared to the timescale of transcription (on the order of several minutes), we can assume reaction 1B is at equilibrium. This implies that $\gamma_{on} T_0 D_0 = \gamma_{off} D_T$. Since $D = D_0 + D_T$ and $T = T_0 + D_T + T_E$ we can rewrite this as equation 5 using the variable $\delta = T_E/T$. Note that we can rewrite the total host-factor level as $T(1-\delta) = T_0 + D_T$ using the relation $\delta = T_E/T$, and the quantity $T(1-\delta)$ is just the total amount of host-factor available for binding to the promoter region of gene X.

$$\gamma_{on}(T(1-\delta) - D_T)(D - D_T) = \gamma_{off} D_T \tag{11}$$

We can multiply out the terms to arrive at a quadratic equation for D_T:

$$T(1-\delta)D - D_T\left(T(1-\delta) + D + \frac{\gamma_{off}}{\gamma_{on}}\right) + D_T^2 = 0 \tag{12}$$

We can solve equation 12 for D_T using the quadratic formula.

$$D_T = \frac{1}{2}\left(T(1-\delta) + D + \frac{\gamma_{off}}{\gamma_{on}}\right) \cdot \left[1 \pm \sqrt{1 - \frac{4DT(1-\delta)}{\left(T(1-\delta) + D + \frac{\gamma_{off}}{\gamma_{on}}\right)^2}}\right] \tag{13}$$

Notice that there are two solutions for the quadratic equation as shown in equation 6. Since we know that $D_T \leq D$ and $D_T \leq T(1-\delta)$, only one solution is plausible and therefore, the final expression for D_T is given by equation 14.

$$D_T = \frac{1}{2}\left(T(1-\delta) + D + \frac{\gamma_{off}}{\gamma_{on}}\right) \cdot \left[1 - \sqrt{1 - \frac{4DT(1-\delta)}{\left(T(1-\delta) + D + \frac{\gamma_{off}}{\gamma_{on}}\right)^2}}\right] \tag{14}$$

Finally, we calculate $f_T = D_T/D$ as in equation 15 (after some rewriting).

$$f_T = \frac{1}{2}\left(\frac{T(1-\delta)}{D} + 1 + \frac{1}{D} \cdot \frac{\gamma_{off}}{\gamma_{on}}\right) \cdot \left[1 - \sqrt{1 - \frac{T(1-\delta)}{D} \cdot \frac{4}{\left(\frac{T(1-\delta)}{D} + 1 + \frac{\gamma_{off}}{D\gamma_{on}}\right)^2}}\right] \tag{15}$$

$$f_T \leq \frac{1}{2}\left(\frac{T}{D} + 1 + \frac{1}{D} \cdot \frac{\gamma_{off}}{\gamma_{on}}\right) \tag{16}$$

From equation 16 we see that as D increases the max possible value of f_T decreases in general. If the amount of host-factor available per gene X is small, then the quantity $z = T(1-\delta)/D$ is small and we can perform a power series expansion in z to determine that f_T is approximated by equation 17 with $\varepsilon = \gamma_{on}/\gamma_{off}$:

$$f_T \approx \frac{T(1-\delta)\varepsilon}{1 + \varepsilon \cdot D} \propto \frac{1}{1 + \varepsilon D} \tag{17}$$

Therefore, equations 16 and 17 tell us that the effective transcription rate depends inversely on DNA copy number. This has the following dependence in general, consistent with equation 7, which we initially proposed:

$$k_{eff} = k_0 f_T \propto k_0 \frac{1}{1 + \varepsilon D} \tag{18}$$

Fold Change formula

We performed a fold-change calculation which serves as a metric to quantify the sensitivity of mRNA levels to the rate of viral DNA replication. The fold change $F(\varepsilon, t)$ is defined as the ratio between i) RNA levels at time t when the replication rate equals a fraction ε of its wild-type value and ii) RNA levels at time t when the replication rate equals its wild-type value. Mathematically, the formula is:

$$F(\varepsilon, t) = \frac{RNA\big(t, r = \varepsilon \cdot r_{opt}\big)}{RNA\big(t, r = r_{opt}\big)}$$

Here r_{opt} is the replication rate determined by parameter optimization. We then calculated the time-average of $\langle F(\varepsilon, t)\rangle$, over all time points (6, 12, 18, 24, 30 and 40 minutes) to indicate the sensitivity of RNA levels to different replication rates.

Parameter Optimization:

The free parameters of this model were determined by fitting to the smFISH data of the λWT and λP^- strains, as well as the average DNA levels over time obtained by qPCR. To optimize the parameters, we defined the cost function as the sum of squared deviations between the model prediction and the experimental data, shown as below:

$$C(\boldsymbol{x}) = \sum_{k=1}^{n} (M_k(\boldsymbol{x}) - \varepsilon_k)^2$$

Here, $\boldsymbol{x} = (x_1, x_2, \dots, x_n)$ is a vector containing the free parameters x_k (24 parameters for the simple model and 29 parameters for the detailed model). ε_k is the k^{th} experimental data point, and $M_k(\boldsymbol{x})$ is the corresponding prediction from the model.

To minimize this cost function, we applied various optimization algorithms including genetic algorithms, particle swarm algorithms, and downhill simplex algorithms. For the purpose of optimizing a stochastic simulation (as is our case), we found that using a random-walk downhill optimization protocol worked best and yielded an optimal solution much faster than the other methods. This random-walk downhill optimization method is described below:

1. Randomly initialize a parameter vector $\boldsymbol{x}$, and calculate the cost function $C(\boldsymbol{x})$.
2. Randomly perturb each element of the parameter vector $x_k \in \boldsymbol{x}$ by generating a random number $r \in (0,1)$ and setting $x_k \coloneqq x_k \cdot \big(1 - p \cdot r + p \cdot (1 - r)\big)$, where p is the "percent-search", e.g., if $p = 0.05$ then we scale x_k up by at most 5% or scale x_k down by at most 5% in each step. We generate a different random number $r \in (0,1)$ for each parameter x_k in $\boldsymbol{x}$. This then defines a new parameter vector $\boldsymbol{x}'$. Score the new parameter vector by calculating $C(\boldsymbol{x}')$.
3. If $C(\boldsymbol{x}') < C(\boldsymbol{x})$, then we move from $\boldsymbol{x}$ to the new point $\boldsymbol{x}'$ by setting $\boldsymbol{x} \coloneqq \boldsymbol{x}'$. Otherwise, we do not move to $\boldsymbol{x}'$ and instead go back to step 2. If we repeatedly go back to step 2 too many times (e.g. higher than some threshold $N_{trials} = 100$), we repeat step 2 but

using a higher p value (e.g. $p = 0.3$) to generate an $\boldsymbol{x}'$ and accept the move even if $C(\boldsymbol{x}')$ is not less than $C(\boldsymbol{x})$. This allows the algorithm to avoid getting stuck in local minima.

4. Terminate the search process if the cost function has been minimized to a desired level.

This algorithm has several advantages compared to the alternative ones mentioned above. It is faster since other algorithms require that the cost function to be calculated many more times per iteration (typically as many times as the number of parameters) before a downhill move is accepted. This method is also robust to incompletely converged cost function calculations. That is, the model's predictions are sample averages from the stochastic simulation. If we want convergent predictions, we must repeatedly run the model thousands or hundreds of thousands of times which slows down the optimization protocol. Ideally, we would want the model's output to be converged within some very small tolerance level, but this is time consuming. It appears that this method still works even if the model's output is not completely converged, which means we can reduce the number of times we must run the stochastic simulation and find minima faster.

Supplemental References

Alvarez, L.J., Thomen, P., Makushok, T., and Chatenay, D. (2007). Propagation of fluorescent viruses in growing plaques. Biotechnol Bioeng *96*, 615-621.

Cortes, M.G., Trinh, J.T., Zeng, L., and Balazsi, G. (2017). Late-arriving signals contribute less to cell-fate decisions. Biophysical Journal *113*, 2110-2120.

Gillespie, D.T. (1976). A general method for numerically simulating the stochastic time evolution of coupled chemical reactions. Journal of computational physics *22*, 403-434.

Gillespie, D.T. (2007). Stochastic simulation of chemical kinetics. Annu Rev Phys Chem *58*, 35-55.

Hoopes, B.C., and McClure, W.R. (1985). A cII-dependent promoter is located within the Q gene of bacteriophage lambda. Proc Natl Acad Sci U S A *82*, 3134-3138.

Howes, W.V. (1965). Protein synthesis in Escherichia coli: a phage-mediated interruption of translation. Biochim Biophys Acta *103*, 711-713.

Jain, D., Kim, Y., Maxwell, K.L., Beasley, S., Zhang, R., Gussin, G.N., Edwards, A.M., and Darst, S.A. (2005). Crystal structure of bacteriophage lambda cII and its DNA complex. Mol Cell *19*, 259-269.

Joh, R.I., and Weitz, J.S. (2011). To lyse or not to lyse: transient-mediated stochastic fate determination in cells infected by bacteriophages. PLoS Comput Biol *7*, e1002006.

Kobiler, O., Rokney, A., Friedman, N., Court, D.L., Stavans, J., and Oppenheim, A.B. (2005). Quantitative kinetic analysis of the bacteriophage lambda genetic network. Proc Natl Acad Sci U S A *102*, 4470-4475.

Lee, C., Kim, J., Shin, S.G., and Hwang, S. (2006). Absolute and relative QPCR quantification of plasmid copy number in Escherichia coli. J Biotechnol *123*, 273-280.

Liu, X., Jiang, H., Gu, Z., and Roberts, J.W. (2013). High-resolution view of bacteriophage lambda gene expression by ribosome profiling. Proc Natl Acad Sci U S A *110*, 11928-11933.

Qian, Y., Huang, H.H., Jimenez, J.I., and Del Vecchio, D. (2017). Resource Competition Shapes the Response of Genetic Circuits. ACS Synth Biol *6*, 1263-1272.

Robb, M.L., and Shahrezaei, V. (2014). Stochastic cellular fate decision making by multiple infecting lambda phage. PLoS One *9*, e103636.

Shao, Q., Hawkins, A., and Zeng, L. (2015). Phage DNA dynamics in cells with different fates. Biophys J *108*, 2048-2060.

Shao, Q., Trinh, J.T., McIntosh, C.S., Christenson, B., Balazsi, G., and Zeng, L. (2017). Lysis-lysogeny coexistence: prophage integration during lytic development. Microbiologyopen *6*.

Shopera, T., He, L., Oyetunde, T., Tang, Y.J., and Moon, T.S. (2017). Decoupling Resource-Coupled Gene Expression in Living Cells. ACS Synth Biol *6*, 1596-1604.

Skinner, S.O., Sepulveda, L.A., Xu, H., and Golding, I. (2013). Measuring mRNA copy number in individual Escherichia coli cells using single-molecule fluorescent in situ hybridization. Nat Protoc *8*, 1100-1113.

Terzi, M., and Levinthal, C. (1967). Effects of lambda-phage infection on bacterial synthesis. J Mol Biol *26*, 525-535.

Trinh, J.T., Szekely, T., Shao, Q., Balazsi, G., and Zeng, L. (2017). Cell fate decisions emerge as phages cooperate or compete inside their host. Nat Commun *8*.

Weitz, J.S., Mileyko, Y., Joh, R.I., and Voit, E.O. (2008). Collective decision making in bacterial viruses. Biophys J *95*, 2673-2680.

Zeng, L., and Golding, I. (2011). Following cell-fate in E. coli after infection by phage lambda. J Vis Exp, e3363.

Zeng, L., Skinner, S.O., Zong, C., Sippy, J., Feiss, M., and Golding, I. (2010). Decision making at a subcellular level determines the outcome of bacteriophage infection. Cell *141*, 682-691.

Zhang, N., and Young, R. (1999). Complementation and characterization of the nested Rz and Rz1 reading frames in the genome of bacteriophage lambda. Mol Gen Genet *262*, 659-667.

Zong, C., So, L.H., Sepulveda, L.A., Skinner, S.O., and Golding, I. (2010). Lysogen stability is determined by the frequency of activity bursts from the fate-determining gene. Mol Syst Biol *6*, 440.